STRAIN RATE EFFECTS ON INELASTIC RESPONSE OF BEAMS

Thesis for the Degree of M. S.

MICHIGAN STATE UNIVERSITY

John G. Janssen

1965

ABSTRACT

STRAIN RATE EFFECTS ON THE INELASTIC RESPONSE OF BEAMS

by John G. Janssen

In this thesis a numerical method for the dynamic analysis of elasto-plastic beams exhibiting strain rate sensitivity is presented. The analysis is based on a discretization of the prototype beam by lumping the mass and flexibility. In order to include the strain rate effect, it is further assumed that the moment curvature relation can be divided into a "static" part and a dynamic part. The static part is based on a bilinear elasto-inelastic relation; the dynamic part is an adaptation of an empirical equation used by Symonds and Ting for considering the strain-rate effects on yield stress for rigid perfectly plastic beams.

The validity of the method presented is proved, for the inelastic case, by establishing the "convergence" of the response of a beam as the discretization becomes finer. For elastic beams, solutions obtained by use of the model are compared with exact analytical solutions. It was shown that, for ten panels, the discrete model predicted a maximum displacement which differs from the exact solution by only 1.2%.

The effect of strain rate was determined by comparing two solutions of the same problem; one considering strain rate, the other

neglecting it. The maximum deflection of a beam of nominal engineering dimensions with no strain hardening subjected to a blast loading was reduced 23% due to the effect of strain rate. However, as the amount of strain hardening increased, the effect of strain rate was reduced.

The method was also used to analyze certain beams that were studied experimentally at Brown University. It was shown that if the strain hardening effects were considered, the results yielded by the discrete model agreed well with the experimental data. The analysis also indicated that as a consequence of the elastic and strain hardening effects an "inelastic rebound" takes place which substantially decreases the permanent deformation of the beams. In this connection the shortcomings of using the rigid perfectly plastic theory to predict the behavior of such beams are pointed out.

STRAIN RATE EFFECTS ON INELASTIC RESPONSE OF BEAMS

by

John G. Janssen

A THESIS

Submitted to
Michigan State University
in partial fulfillment of the requirements
for the degree of

MASTER OF SCIENCE

Department of Civil Engineering

1965

ACKNOWLEDGMENTS

The author would like to express his gratitude to his advisor, Dr. Robert K. Wen, whose advice and assistance proved to be invaluable during the course of this study. Thanks are also due to Dr. Charles Cutts, Chairman of the Department of Civil Engineering, for his encouragement.

Special thanks are extended to the National Science Foundation and to the Division of Engineering Research, for their support which made this work possible. Also the personnel of the Computer Laboratory are deserving of thanks for their advice and cooperation during the course of this study.

And last but not least go thanks to the author's wife, Sue, whose encouragement during many difficult periods was genuinely appreciated.

TABLE OF CONTENTS

LIST OF TABLES

LIST OF FIGURES

CHAPTER I

INTRODUCTION

1.1 General

In recent years the problem of the dynamic response of inelastic beams and frames has been the subject of many technical papers. The nonlinear aspects of the problem and the inherent complexities of structural systems preclude "exact" solutions to all but the simplest problems. Because of this, analysts have been forced to make certain assumptions which transform or simplify their original problems into more manageable ones.

One mode of simplification is to reduce the continuous nature of the problem to a discrete one. This is particularly attractive today as the ensuing large amount of numerical work (a serious drawback of such an approach in yesteryear) can now be handled conveniently by the electronic computer. The mathematical model associated with the discretized system will be referred to as the discrete model in this thesis.

Wen and Toridis (13)* have investigated three discrete models for inelastic beams. It was shown that quite accurate results (as compared to available solutions of continuous systems and experiments) could be obtained by use of the discrete models. The major advantage

*Numbers in parentheses refer to references listed in the bibliography.

of the method is that it can be conveniently used to predict the response of quite general structural configurations and loadings and, even though a computer is generally needed, the application and programming are quite straightforward.

The majority of past works done in the area of structural dynamics have neglected the effect of strain rate on the response of the structure. It is generally known, however, that some materials exhibit an increase in their yield stress while under dynamic loading conditions. This effect on the bending of beams has been studied at Brown University by Bodner and Symonds (1), who ran tests on small cantilevers subjected to impulsive loadings. They also undertook a mathematical analysis in which the analytical representation of the strain rate effects was based on experiments carried out by Manjoine (4).

Other researchers at Brown University (5, 12) as well as Parkes (8, 9) in England have also studied the effects of strain rate on the response of simple structures. In all the analytical works mentioned above it was assumed that the material exhibits a rigid perfectly plastic moment curvature relationship; thus, the effects of the elastic response and possible strain hardening were neglected. Therefore, in order for their analysis to be meaningful, the inelastic deformation must be of a much greater order of magnitude than the elastic deformation. This restriction upon the rigid perfectly plastic theory limits the range of applicability in many practical situations. Also their methods of analysis, though capable of treating simple structural elements such as cantilever beams, do not in general seem adaptable to complex structural systems.

Since the discrete model approach is applicable to a wide range of material properties and complicated structural configurations (see for example, reference 14) it is natural to attempt to extend it to include the effects of strain rate in addition to the elastic, plastic, and strain hardening properties.

1.2 Scope

The present investigation begins with the formulation of the moment curvature relation that incorporates both strain-rate and strain hardening effects. Next, a method of analysis is developed for computing structural response. Numerical results are then obtained for a number of problems all involving cantilever beams. This was done because: (i) the results could thus be compared with existing continuous solutions and experimental data, and (ii) since the method is obviously readily applicable to more complex structures, no numerical demonstration of such applications are deemed necessary.

The accuracy of the method is demonstrated by (i) comparing a known exact solution for the completely elastic case to results obtained by use of the model, (ii) showing that as the number of divisions of the model is increased, the solutions seem to approach a limit, and (iii) comparing results obtained with the model to experimental results and continuum solutions given in reference (1).

Having (reasonably) established the reliability of the model, numerical results are then obtained to study the influence of strain rate and strain hardening.

1.3 Notations

The following symbols and notations have been used in this thesis and are listed below in alphabetical order.

A_n	=	constant
A_y	=	area of cross section that has yielded
a	=	thickness of flange of WF section
B_n	=	constant
B_o	=	constant
b	=	width of flange of WF section
C_n	=	constant
c	=	constant
D	=	constant with dimension of 1/sec
d	=	depth of WF section
dt	=	time increment
E	=	modulus of elasticity
$\dot{e}$	=	strain rate
G	=	mass of tip of beam
G_n	=	constant
h	=	panel length

I	=	moment of inertia
I_o	=	impulse
i, n, m	=	subscripts
K_1	=	elastic stiffness
K_2	=	inelastic stiffness
k	=	curvature
k_o	=	curvature at intersection of elastic line with curvature axis
$\acute{k}$	=	curvature rate
L	=	length of beam
M	=	bending moment
M_i	=	internal bending moment of beam at ith joint
M_l	=	lower bound of "static" elastic action
M_o	=	"static" moment at which beam initially behaves inelastically
M_{sr}	=	moment due to strain rate (or curvature rate)
M_{tl}	=	total moment, lower ($M_{sr} + M_l$)
M_{tu}	=	total moment, upper ($M_{sr} + M_u$)
M_u	=	upper bound of "static" elastic action
$\bar{M}_{sr}$	=	M_{sr}/M_o
m_i	=	mass lumped at panel point i
$m(x)$	=	mass distribution of beam
N	=	number of panels beam is divided into
$P_i(t)$	=	load lumped at panel point i
p	=	constant

p	=	angular beam frequency (in Appendix only)
p(x,t)	=	loading function of beam
Q	=	ratio of kinetic energy input to maximum storable elastic energy $(I_o^2/2G)/(M_o^2L/2EI)$
R	=	ratio of stiffnesses, K_2/K_1
RK	=	G/mL
r	=	constant
S_a	=	assumed section modulus
S_e	=	elastic section modulus
S_p	=	plastic section modulus
T_n	=	period of nth mode of beam
T_1	=	first fundamental period of simply supported beam
t	=	time
V_o	=	initial velocity of tip
V_i^+	=	internal shear to the right of the ith joint
V_i^-	=	internal shear to the left of the ith joint
w	=	uniform load in #/ft.
w_e	=	load which causes extreme fibers to yield
X(x)	=	mode shape of a slender prismatic beam
x_i	=	location of ith joint from the left support
x'	=	point midway between the (ith-1) and the ith joint
x''	=	point midway between the ith and the (ith+1) joint
y(x,t)	=	deformation curve of beam
y_i	=	deflection of the ith joint

$\dot{y}_i$ = velocity of the ith joint

$\ddot{y}_i$ = acceleration of the ith joint

z = distance from neutral axis of beam

σ_o = initial static yield stress

σ_{sr} = stress due to strain rate

$\bar{\sigma}_{sr}$ = ratio of σ_{sr} and σ_o

σ_y = dynamic yield stress

θ_i = joint rotation

$\dot{\theta}_i$ = rotation rate

λ = mp^2/EI

$\psi_n(t)$ = generalized coordinate

CHAPTER II

FORMULATION OF MOMENT CURVATURE RELATION

2.1 Basis of Moment Curvature Relation

For the most part the moment curvature relation used in connection with this work is that of the bilinear type with a modification included to incorporate the effect of strain rate. The dynamic moment curvature relation is assumed to be the sum of the "static" moment curvature relation and the effects due to strain rate.

Consider the moment curvature diagram of a beam cross section which is being loaded slowly. The effect of strain rate will be considered negligible in this case. The moment curvature diagram under consideration has two distinct parts. The first part, which shall be called the elastic line, is represented in Figure 2.1 by the line

$$M = K_1(k - k_o) \tag{2.1}$$

where M is the bending moment, K_1 is the elastic stiffness, k is the curvature, and k_o is the intersection of the elastic line with the curvature axis. The second part, which will be called the inelastic line, is represented by one of the lines

$$\left.\begin{aligned} M_u &= K_2 \cdot k + B_o \\ &\text{or} \\ M_l &= K_2 \cdot k - B_o \end{aligned}\right\} \tag{2.2}$$

depending on the direction of the inelastic bending. The constant B_o

represents the M intercept of the inelastic lines, and K_2 is the inelastic stiffness. When inelastic straining takes place, Equation (2.1) (the elastic line) is adjusted to take care of the hysteresis effect by changing k_o by the amount of the inelastic straining. For the virgin case, k_o is equal to zero.

The two inelastic lines represented by Equations (2.2) do not shift as does the elastic line. These lines are considered the upper and lower bounds of the static flexure strength of the cross section. The constant B_o in the equations depends on the slope of the inelastic lines and the yield moment M_o. With the moment curvature relation of the static case as a foundation, the consideration of the effect of strain rate on the characteristics of the beam follows.

Let M_{sr} denote the increase in the yield moment due to strain rate. While its formulation involving the strain (or curvature) rate will be given in the next section, its relation to the overall moment curvature relation is discussed here.

It will be assumed that the rate of straining will have no effect upon the elastic portion of the moment curvature relation. Furthermore, it will be assumed that the absolute value of the section can be no more than that given by Equation (2.1) to account for the strain history. Since the yield moment for a given section depends upon its rate of curvature as well as its curvature, the value of the yield moment will, in general, vary with time.

Knowing the curvature and the curvature rate at any cross section the yield moment at that cross section may be determined by adding the increase in yield moment due to strain rate and the "static" yield moment. Therefore the yield curve is represented by Equations (2.3)

$$\left.\begin{aligned} M_{tu} &= M_u + M_{sr} \\ M_{tl} &= M_l + M_{sr} \end{aligned}\right\} \quad (2.3)$$

where M_{tu} and M_{tl} represent, respectively, the total upper and lower yield moments.

In Figure 2.2 is shown a moment curvature diagram of a strain rate sensitive cross section. The representation differs from the static case in the inelastic region only. For example, yielding takes place at point A for the static case, while for the dynamic case, the yield point continues to move up the elastic line until it reaches point A', after which it moves along the yield line to point C. Point C is the point where there is a reversal of the direction of straining. At that point the strain rate is zero, and the yield line and the inelastic line intersect. The configuration point will then move down an elastic line to point D.

2.2 Formulation of M_{sr}

Manjoine (4) has conducted experiments to find the effect of strain rate on yield stress. Tests were run at various strain rates and temperatures and one set of tests was run at room temperature. From this data Ting and Symonds (12) have derived a relationship between yield stress and strain rate as follows:

$$\dot{e} = D\left(\frac{\sigma_y}{\sigma_o} - 1\right)^p \tag{2.4}$$

where $\dot{e}$ is the strain rate, σ_o is the initial static yield stress, σ_y is the yield stress corresponding to $\dot{e}$, and D and p are constants determined from Manjoine's work. Figure 2.3 shows the effect of strain rate on the yield stress of aluminum and steel. The values for mild steel were due to Manjoine and those for aluminum to Parkes (8).

It is desirable to have the constitutive equations given in terms of moment and curvature rate rather than stress and strain rate since it is moment and curvature that will be used in the analysis. Equation (2.4) can be written in the form

$$\dot{k}z = D(\bar{\sigma}_{sr})^p \tag{2.5a}$$

where $\dot{k}$ is the curvature rate, z is the distance from the neutral axis to the fiber in question and

$$\bar{\sigma}_{sr} = \frac{\sigma_y - \sigma_o}{\sigma_o} = \frac{\sigma_{sr}}{\sigma_o}$$

By inverting Equation (2.5a), Equation (2.5b) results

$$\bar{\sigma}_{sr} = \left(\frac{\dot{k}z}{D}\right)^{1/p} \tag{2.5b}$$

To determine the percentage increase in moment, $\bar{M}_{sr} = M_{sr}/M_o$, all that is necessary is to integrate the moment of $\bar{\sigma}_{sr}dA_y$ over the cross section;

$$\bar{M}_{sr} = \int_{A_y} z\,\bar{\sigma}_{sr}\,dA_y/[M_o] \tag{2.6}$$

where A_y is that area of the cross section which has yielded.

If a wide flange section is considered, it is reasonable to assume that only the flanges resist bending and that the stress distribution over the flange is constant (see Figure 2.4). Under the slightly conservative assumption, z = constant = d/2, Equation (2.6) becomes

$$\bar{M}_{sr} = a\,b\,d\left(\frac{\dot{k}\,d}{2D}\right)^{1/p} \qquad (2.6a)$$

where a, b, and d are as defined in Figure 2.4.

CHAPTER III

METHOD OF ANALYSIS

3.1 Introduction

The beam is assumed to deform by bending only. The prototype that the discrete model is to represent has continuous distributions of mass and flexibility. Figure 3.1a shows the general beam of this type with a continuous loading. In general, the flexibility, mass and loading may vary with the distance along the beam. Also, the loading may vary with time. Any practical support conditions may be considered. Free, fixed, and simple supports are illustrated in the figure. Motion of the supports, as in an earthquake, can be easily considered.

3.2 Discretization

The model of the prototype beam is derived by dividing the prototype beam into rigid, massless "panels." At this point it is convenient, although not necessary, to consider that the beam is divided into N panels of equal length, h. The mass and loading of the prototype beam are lumped in a tributory manner at the flexible joints between two panels. Consider the joint, i, in Figure 3.1b. The mass at i is obtained by summing the mass of the prototype between x' and x'' where $x' = x_i - h/2$, and $x'' = x_i + h/2$. Then the mass at joint i is given by Equation (3.1).

$$m_i = \int_{x'}^{x''} m(x)\, dx \qquad (3.1)$$

In which m(x) is the mass distribution per unit length. The load at joint i is obtained in a similar manner.

$$P_i(t) = \int_{x'}^{x''} p(x,t)\,dx \qquad (3.2)$$

To determine the flexibility of joint i, consider that the curvature of the beam over the interval from x' to x'' is given by $k(x_i)$, the curvature at x_i of the prototype beam. The rotation of the joint is given by integrating the curvature over the interval x' to x''.

$$\theta_i = \int_{x'}^{x''} k(x_i)\,dx$$

$$= k(x_i)(x'' - x')$$

$$\theta_i = hk(x_i) \qquad (3.3)$$

From Figure 3.1c θ_i may be determined from consideration of the geometry of the system.

$$\theta_i = \frac{1}{h}(y_i - y_{i-1}) + \frac{1}{h}(y_i - y_{i+1})$$

$$\theta_i = -\frac{1}{h}(y_{i-1} - 2y_i + y_{i+1}) \qquad (3.4)$$

From Equation (3.3) it is noted that by multiplying the abscissa of the moment curvature diagram by h, it will be converted to a moment-joint rotation diagram. Since the yield stress of the beam being studied exhibits rate dependent characteristics, the rate of joint rotation must be related to the curvature rate so that the yield moment may be determined. By taking the time derivatives of Equations (3.3) and (3.4), a relationship between the joint rotational velocities and the curvature rate is found and the yield moment may be determined as shown in Chapter II.

$$\begin{aligned} \dot{\theta}_i &= h\dot{k}(x_i) \\ \dot{\theta}_i &= -\frac{1}{h}(\dot{y}_{i-1} - 2\dot{y}_i + \dot{y}_{i+1}) \end{aligned} \tag{3.5}$$

Thus, the rotations of the joints are defined in terms of the joint displacements.

It should be noted that the above formulas are valid only for small deformations. However, it was found that for certain problems involving an initial tip velocity of a cantilever beam (see sections 4.1 and 5.1), these formulas also yield sufficiently accurate results for the angular deformations at the tip.

3.3 Equations of Motion

The equations of motion for the beam may be determined by considering a free body diagram of joint i (see Figure 3.1d). V_i^+ is the shearing force to the right of the joint, V_i^- is the shearing force to the left, $\ddot{y}_i$ is the acceleration of the joint, positive downward, and the M_i's are the moments at the joints. Using Newton's second law of motion and taking downwards as positive, Equation (3.6) is obtained.

$$m_i\ddot{y}_i = V_i^+ - V_i^- + P_i(t) \tag{3.6}$$

The shearing forces, V_i's, may be expressed in terms of moments at joints by applying the laws of statics to the massless panels.

$$\begin{aligned} V_i^+ &= \frac{1}{h}(M_{i+1} - M_i) \\ V_i^- &= \frac{1}{h}(M_i - M_{i-1}) \end{aligned} \tag{3.7}$$

Substituting (3.7) into (3.6) one obtains:

$$m_i \ddot{y}_i = \frac{1}{h}(M_{i-1} - 2M_i + M_{i+1}) + P_i(t) \tag{3.8}$$

There will be an equation similar to Equation (3.8) for each joint that is free to move in the y direction.

3.4 Support Conditions

The effects of the support conditions on the equations of motion and flexibility are not difficult to determine. For example, V^+_{N+1} and M_{N+1} would be equal to zero for a free end. The flexibility of a joint at a fixed end would not be the same as that for the rest of the joints. This is because there is only one-half of a panel to contribute to the flexibility. Consider the fixed end at joint No. 1 in Figure 3.1b. The rotation and angular velocity are given by:

$$\begin{aligned} \theta_1 &= \frac{h}{2} k(0) = y_2/h \\ \dot{\theta}_1 &= \frac{h}{2} \dot{k}(0) = \dot{y}_2/h \end{aligned} \tag{3.9}$$

Therefore, in order to use the same moment rotation relationship that is used for the interior joints, the angle of rotation at a fixed end must be multiplied by 2.

3.5 Numerical Integration of Equations of Motion

The response of the model is determined by a step by step numerical integration procedure. The $\beta = 0$ method, as outlined in reference (7), is used in this study. If $y_i(t)$, $\dot{y}_i(t)$ and $\ddot{y}_i(t)$ are, respectively, the displacement, velocity and acceleration of the ith joint at time t, and $\ddot{y}_i(t+dt)$ is the acceleration at time t + dt, then the displacement and velocity at t + dt is given by

$$\left.\begin{aligned} \dot{y}_i(t+dt) &= \dot{y}_i(t) + \frac{1}{2}\,dt\,[\ddot{y}_i(t) + \ddot{y}_i(t+dt)] \\ y_i(t+dt) &= y_i(t) + dt\,\dot{y}_i(t) + \frac{1}{2}\,dt^2\,\ddot{y}_i(t) \end{aligned}\right\} \quad (3.10)$$

It should be noted that $\ddot{y}_i\,(t+dt)$ is in general unknown. Thus an iterative procedure is necessary. A typical step will now be explained.

1) At time t, the beginning of the step, the displacements, velocities and accelerations are known.

2) The acceleration at the end of the step, time = t +dt, is assumed equal to the acceleration at time equal to t.

3) The velocities and displacements at the end of the step can now be computed by Equations (3. 10).

4) The configuration of the system at the end of the step is now known, so that from geometry the rotations of the joints can be determined along with the rate of rotation. From the moment joint rotation relationship and the effect of rotation rate, the moment at each joint can be determined. Then by Equations (3.8) the accelerations at the end of the step can be determined.

5) These new accelerations are compared with the values assumed in part (2). If the new and old sets of values are within an allowable tolerance, the iteration is said to have converged.

6) If, at the end of the try, the assumed acceleration does not agree with the acceleration found in part (4) to within an allowable tolerance, the iteration has not converged and another value for the acceleration at time = t+dt must be assumed. This new assumed acceleration is taken as the acceleration found in part (4) of the previous try. Steps (3) to (6) are repeated until the iteration converges.

7) If the iteration has converged, the time is advanced by the time increment, dt.

8) The displacements, velocities, and accelerations found at the end of this step become the initial conditions for the next step.

In passing, it may be mentioned that the convergence of the $\beta = 0$ method of numerical integration is automatic if the quantities in the equation of motion do not depend on the velocities at the end of a "try." Otherwise, iteration is required.

According to reference (7) the time increment for each step must be less than $1/\pi$ times the smallest period of vibration to insure stability of the numerical procedure. If the number of panels into which the beam is divided is relatively large, the smallest period of vibration, T_n, of a beam with arbitrary conditions may be approximated by

$$T_n = T_1/N^2 \tag{3.11}$$

where T_1 is the fundamental period of a simply supported beam of the same length and cross section, and N is the number of panels (see reference 13). The time interval used in this study is given by

$$dt = \frac{1}{4} T_1 / N^2 \qquad (3.12)$$

CHAPTER IV

NUMERICAL RESULTS

4.1 Description of Problems

All the numerical data presented herein pertain to cantilever beams. However, two types of beam load systems were considered. In the first case, the numerical values of the parameters of the problem are quite realistic; i.e., they correspond to I-beams subjected to blast loading. The objective of obtaining these data was to get some idea about the engineering significance of the variables considered, i.e. strain rate and strain hardening.

The second type of problem deals with a somewhat more academic case of a rectangular slender beam with a heavy tip mass subjected to a tip impulse load. The motivation for considering this problem was that it had been studied by other investigators and the results could thus be compared.

Figure 4.1a shows the prototype cantilever beam with a uniform load, and Figure 4.1b shows the corresponding discrete model for N = 10. The static moment curvature diagram for a 10WF66 beam is shown in Figure 2.4. The value of the section modulus, S_a, is taken to be a b d, where a, b, and d have been defined in Figure 2.4. This value is conservative in the plastic range and is a reasonable compromise between the elastic section modulus and the fully plastic section modulus. The load on the beam is given by

$$w = cw_e e^{-rt} \tag{4.1}$$

where $w_e = 2\sigma_o S_a / L^2$ is the static elastic limit load, t is the time, and c and r are numerical constants which determine the magnitude and duration of the loading.

For the second problem the prototype beam is shown in Figure 4.2. The general problem consists of a cantilever beam with a relatively "limber" cross section and a large concentrated tip mass. An impulsive load is applied on the tip so as to give the mass an initial velocity

$$V_o = I_o / G$$

where V_o is the tip velocity, I_o is the impulse applied to the tip, and G is the mass of the tip.

4.2 Accuracy of the Model

Before any remarks are made about the dynamic response of the beams studied in this paper, the accuracy of the discrete model used must first be considered. The model, being composed of discrete points where mass and flexibility are lumped, is only an approximation to the continuum prototype beam. However, as the number of panels is increased and the divisions of the beam become finer, it would be expected that the model would more closely approximate the prototype beam. In the limit, with the number of joints approaching infinity, the model would approach the prototype.

To show this "convergence," a cantilever beam with an attached tip mass subjected to an impulse loading is analyzed for stiffness ratios of R = 0 and R = 0.1, where R is the ratio of the inelastic stiffness to the elastic stiffness. For the convergence of the model for R = 1.0, a cantilever beam subjected to a suddenly applied uniform load is used. The data are presented in Figures 4.3 and 4.4 which are graphs of the maximum dimensionless displacement versus the reciprocal of N. In each case, the results are seen to approach an "apparent limit" as N increases.

By comparing Figures 4.3 and 4.4 with Figures 10, 11, 12, and 13 of reference (13) (which deals with simply supported beams) it will be noted that the convergence is of a similar nature. For each value of R the model converges to an apparent limit as N becomes larger. However, the model converges faster for larger values of R.

The value of R = 1.0 corresponds to the case of a perfectly elastic beam. For this case an exact analytical continuum solution is obtainable and is presented in the Appendix. Figure 4.5 is a graph of tip deflection (scaled by the static yield deflection = $2\sigma_o L^2/3Ed$) versus time for a cantilever beam subjected to a suddenly applied uniform load. The response curves are shown for the exact continuum solution as well as the discrete solutions corresponding to N = 10 and N = 20. It can be seen that the response curves of the discrete model are very close approximations to the continuum case. Also the convergence of the discrete case can be noted by the fact that N = 20, more nearly approximates the exact case than does N = 10 (even though they are both very good). For the case of a uniform load which is suddenly applied and then decreases exponentially with time, similar results were obtained and are not presented herein.

Although theoretically it appears that by taking increasingly larger values of N, the discrete model may be made as accurate as the analyst wishes, however, a point of diminishing returns would be reached when round off error and computer time consumption make the use of a larger value of N unrewarding. For the purposes of this thesis the value of N = 10 seems to be a good choice. The accuracy obtained is sufficient and the amount of computer time used is quite modest (about 2 minutes for an average problem with N = 10).

4.3 The Effect of Strain Rate

In order to study the effect of strain rate on the dynamic response of beams a comparison is made between two identical beams under identical loadings. The only difference between the two beams is that the analysis of one of the beams considers strain rate while the analysis of the other neglects it.

Since strain rate has the effect of increasing the yield moment, it is natural to expect that the magnitude of response of a strain rate sensitive beam would be reduced. This is indeed the case. The reduction for the particular beam under consideration was of the order of 23%

for R = 0 (see Figure 4.8). This reduction, of course, would depend upon the sensitivity of the material to strain rate and the amount of plastic action undergone.

The effect of the length of the beam seemed to have little effect on the dimensionless deflection (see Figure 4.6). By shortening the beam the frequency of elastic vibration is increased in proportion to $1/L^2$ and since strain rate is proportional to the frequency it would seem natural that there should be a still larger reduction due to strain rate sensitivity. But this was not found to be the case. Similarly, altering the rate of straining did not noticeably change the percent reduction of the deflection for the strain rate sensitive case. An explanation for these two seemingly puzzling facts can be found by an examination of Equation (2.6a). Taking the derivative with respect to $\dot{k}$:

$$\frac{d\bar{M}_{sr}}{d\dot{k}} = \frac{\bar{M}_{sr}}{p\dot{k}} \tag{4.3}$$

It is seen that the rate of increase of the yield moment decreases with an increase in strain rate. That is, the higher the strain rate, the more insensitive is the beam to strain rate. Mentel (7) has made a similar observation with regard to the effect of strain rate on yield moment.

4.4 Effect of Strain Rate in the Presence of Strain Hardening

In Figure 4.7 is plotted the dimensionless maximum tip deflection of a cantilevered beam versus the ratio of the inelastic (strain hardening) stiffness to the elastic stiffness, R, for the cases of strain rate considered and strain rate neglected. The beam has a wide flange cross-section and is subjected to a dynamic load of the type given by Equation (4.1).

The effect of strain hardening is to reduce the maximum deflection of the beam, which is to be expected. It is of notable importance that for small values of R, a small variation of it will cause a considerable change in the maximum deflection. For the strain-rate-neglected analysis, a change from R = 0 to R = 0.05 has approximately the same effect as a change from 0.05 to 0.5, or a change from 0.1 to 1.0 (see Figure 5.3 for relative magnitudes of the maximum elastic and inelastic strains corresponding to the data R = 0 plotted in Figure 4.7). Since strain hardening is an inelastic phenomenon, the effect it has will of course depend upon the amount of inelastic deformation the beam will undergo. For example, if there is no inelastic action, then the effect of strain hardening is unimportant. On the other hand, if the amount of inelastic action is much greater than the elastic action, the role of strain hardening may be very important and a value of R = 0.02 or 0.04 can be significant (see Figure 4.9). When strain rate is considered along with strain hardening, an even greater reduction in maximum deflection is noted. As mentioned before, for R = 0, strain rate had the effect of reducing the maximum tip deflection by 23% as compared to the strain-rate-neglected case (see Figure 4.8). However, as the value of R is increased the effect of strain rate is reduced. Since the effect of strain rate takes place in the plastic range only, it is not surprising that, for R = 1.0 (the perfectly elastic case), no effect at all is noticed.

It is interesting to consider how these two material properties affect one another. On examination of Figure 4.7 it is noticed that the curve which represents the strain-rate sensitive case is flatter than the rate-insensitive curve. This indicates that the strain rate moderates the effect of strain hardening. However, the difference between the two cases becomes less with increasing strain hardening. This, in turn, indicates that strain hardening also moderates the effect of strain rate.

In Figure 4.9 is plotted the response history curves of similar beams subjected to the same loading by having stiffness ratios varying from R = 0 to R = 0.05. This could give a better insight into the effect of strain hardening on the response for small values of R. Along with the reduction of the maximum deformation (the tip end slope is being used as a measure of deformation in this case) there is also a reduction in the final permanent set, taken to be the configuration corresponding to zero moments, and in the time required to reach the maximum deformation. The reduction in the permanent set is, in general, greater than that in the maximum deformation.

CHAPTER V

COMPARISON OF DISCRETE SOLUTIONS WITH EXPERIMENTS AND CONTINUUM SOLUTIONS

5.1 Description of Experiments

A comparison of the results obtained by the method of analysis presented in this work and experiments carried out at Brown University (1, 5 and 12) has been made in an attempt to discuss the validity of this method. A detailed account of the experiments and a table of the results are presented in references (1) and (5). Along with the experimental results, a method of analysis based on a "rigid plastic" theory is also presented in these references.

In general, the experiments were carried out on cantilever beams with relatively large concentrations of mass at their tips. A high energy impulse load was applied to the tip mass; the resulting deformations and permanent sets were generally quite large. Tests were run on steel and aluminum beams with two varieties of each type of metal. A summary of some of the tests and results is given in Table (1) of this work.

5.2 Rigid Plastic Continuum Analysis

The theory presented in the above mentioned references is based upon the assumption that the material has a rigid plastic bending moment-curvature relation. This assumption requires that until the bending moment reaches M_o the "yield moment," the beam cross section remains rigid, i.e., there will be no curvature or straining. When M_o is reached, the curvature can be indefinitely large. By assuming the rigid plastic property, a mathematical analysis, treating the beam as a continuum, became feasible. Two versions of such analyses were proposed. Symond's (1) rate sensitive solution is based upon the conservation of momentum principle. The equations of conservation of linear momentum and conservation of angular momentum must then be solved by numerical integration. Ting's (see reference 1) rate sensitive solution is an approximation since the "damage" angle is obtained by multiplying the rate insensitive "damage" angle by an appropriate constant. The constant is determined by considerations of material properties, mass distribution and loading.

Since the model used is continuous, the curvature rate at every point along the beam is defined. The increase in yield stress at every point along the beam can then be determined. It is, however, necessary to use a numerical method - an iterative procedure - to obtain the effect of curvature rate, since the rate of curvature and the moment are inter-dependent. However, as discussed previously small changes in strain rate do not significantly affect the yield stress; hence, the iterative procedure converges rapidly.

5.3 Analysis by the Discrete Model

In order to analyze, by use of the discrete model, the systems studied experimentally, it was necessary to make certain assumptions regarding the physical properties of the systems. Following the lead of the experimenters, the fully plastic moment for the rectangular beam was taken as 1.5 times the extreme fiber yield moment. The end or tip mass was assumed to be concentrated at the last mass point of the model. Neither rotary inertia nor shear effects have been considered. Effects of geometry changes are also neglected (geometry effects are not too important even though the deflections are quite large).

5.4 Comparison of Experimental and Analytical Results

A summary of the experimental results and analytical results obtained from references (1, 5 and 12) along with the results based on the discrete model is presented in Table (1). As mentioned before, the deflections and permanent sets are quite large. The symbol Q (Q corresponds to R in reference 1) given in the table represents the ratio of the total energy absorbed to the maximum elastic energy ($M_o^2 L/2EI$) which can be stored in the beam. For the beams listed in Table (1), the value of Q ranges from about 3 to 16, which indicates that, for the cases under consideration, plastic action generally dominates the behavior.

For the case of R = 0, the discrete model gives rotations which are consistently larger than the experimental values. The differences are larger for the steel test samples, and smaller for the aluminum samples. In an attempt to explain them, the assumption of R = 0 is examined. It is felt that for the magnitude of deformation involved in the tests (for example, 0.10 in/in strain for sample E4, reference (1), should be well into the strain hardening range) the influence of strain hardening may be important. Since the deformations and strains are large enough to cause strain hardening in the steel samples the data was analyzed considering strain hardening. Reference (6) gives the ratio of the elastic modulus to the strain hardening modulus to fall into the range from 20 to 50. This corresponds to a range of R values from 0.02 to 0.05. A value of 0.04 was chosen for the value of R in the calculations. Since aluminum does not exhibit strain hardening to the degree that steel does, a value of the stiffness ratio of 0.01 was chosen for aluminum. For these values of R the discrete model yields results that agree quite closely to the experimental values as shown in Table (1).

The analytical results presented by the experimenters compare favorably with the experimental results, more favorably than those yielded by the discrete model with R = 0. However, when strain hardening is considered the discrete model does as well, and sometimes even better than the experimenters' analysis. It is worthy of note that the deformations are rather sensitive to the small value of R used. This and some other aspects of the problem will be further examined in the following section.

5.5 Discussion of Behavior for Different Material Properties

It is obvious that elastic vibrations cannot be considered in the rigid perfectly plastic solutions. However, for some of the samples, elastic deformations amounted to about 18% of the maximum deflection. Strain hardening, which is also neglected in rigid plastic solutions, was considered in reference (5) to have an effect of 15% of the maximum deflection. It seems that a combination of these two items, strain hardening and elastic action, could significantly influence the behavior.

For simplicity, let the beam be represented by a system with a single degree of freedom as shown in Figure 5.1a. Consider the moment rotation diagrams shown in Figure 5.1 for the rigid perfectly plastic case. Since the response would not include elastic vibrations, once the yielding has ceased no other motion would exist. For the elasto-perfectly plastic case, shown in Figure 5. 1c, however, there could still be motion after plastic action had stopped. This motion could consist of elastic vibrations about the equilibrium position represented in Figure 5.1c by moving back and forth along line AB.

This elastic vibration when coupled with strain hardening would lead to the existence of an "inelastic rebound," explained as follows. In Figure 5.1d is shown a moment rotation diagram which considers elastic action and strain hardening. Assume that the section has undergone inelastic bending such that point A gives the configuration of the cross section on the moment rotation diagram. The area ABC corresponds to the elastic energy stored in the beam. This energy will be converted into kinetic energy as the configuration crosses the rotation axis. This kinetic energy must in turn be absorbed by the beam by a combination of elastic and inelastic deformations. Area BDEF corresponds to this energy. Now the only elastic strain energy remaining is that corresponding to the area EFG. Thus, deformation BG corresponds to the inelastic rebound.

In Figure 5.2 is shown the moment joint rotation history curve for joint #1 plotted from computer results. These results correspond to the analysis of sample E4 assuming a value of R = 0.05. It can be seen that the "inelastic rebound" has reduced the permanent deformation by more than 50% of the maximum deformation. It is apparent that inelastic rebound can occur only when both elastic action and strain hardening enter into the behavior.

Another interesting feature exhibited in Figure 5.2 is the saw tooth shape of the graph. This is caused by the strain rate effects. Since only the results of every fiftieth step of integration were printed out by the computer, the intermediate values can only be guessed at. However, in Figure 5.3 is shown the moment joint rotation history curve of joint #1 of a cantilever beam with R = 0. In this case the value of moment and joint rotation for every step was printed out by the computer. The saw tooth effect is seen to be more pronounced than in Figure 5.2. This effect is thought to be caused by the presence of higher modes which, in turn, cause the velocity of rotation to be uneven and to change rapidly from plus to minus. When a change of sign of velocity occurs, the moment due to strain rate goes to zero; any subsequent increase in moment would follow an elastic line with an appropriate new value of k_o (Equation 2.1). Thus, the "saw tooth" shape results.

In cases where the inelastic action of a structure is only moderate compared to the elastic action, the rigid perfectly plastic approach would be at a disadvantage since the elastic effect is not negligible. If, on the other hand, the inelastic action is large enough to warrant neglection of the elastic action, strain hardening would probably be present to a substantial degree. This also limits the range of applicability of the rigid plastic theory.

CHAPTER VI

CONCLUSIONS

The method of analysis presented in this thesis can consider bilinear elasto-plastic moment curvature relations which incorporate strain hardening and strain rate effects. Based upon the data and discussions presented, it is reasonable to conclude that this method does, to a good degree of accuracy, predict response of structures. Since the method is based upon a discrete model, it may be applied to very general structural configurations such as frames (see reference 14).

In comparing the present method of analysis with past works based on a rigid plastic theory, it is pointed out that although the latter theory enables the analyst to use a continuum model, the features which it neglects may be too important. For example, this theory cannot produce the "inelastic rebound" phenomenon which, as discussed earlier, plays an important part in the response picture.

The results of the investigation indicated that the behavior under consideration is very sensitive to the shape of the moment curvature curve. It would, therefore, seem desirable as a possible future extension of this work, to try a more nearly correct approximation to the "true" moment curvature relation than the bilinear one used here.

VII. BIBLIOGRAPHY

1. Bodner, S. R., and Symonds, P. S., "Experimental and Theoretical Investigation of the Plastic Deformation of Cantilever Beams Subjected to Impulsive Loadings," Journal of Applied Mechanics, Vol. 29, No. 4, December 1962, pp. 719-728.

2. Heidebrecht, Arthur C., Lee, Seng-Lip, and Flemming, John F., "Dynamic Analysis of Elastic-Plastic Frames," Journal of the Structural Division, ASCE, Vol. 90, No. ST2, Proceedings Paper 3881, April 1964, pp. 315-343.

3. Hodge, Philip G., Plastic Analysis of Structures, New York: McGraw Hill and Co., 1959.

4. Manjoine, M. J., "Influence of Rate of Strain and Temperature on Yield Stresses in Mild Steel," Journal of Applied Mechanics, Vol. 11, No. 4, 1944, pp. 211.

5. Mentel, T. J., "Impact Deformation of a Cantilever Beam," Journal of Applied Mechanics, Vol. 25, No. 4, December 1958, pp. 515.

6. Neal, B. C., The Plastic Methods of Structural Analysis, London: Chapman and Hall Ltd., 1956.

7. Newmark, N. M., "A Method of Computation for Structural Dynamics," Transactions, ASCE, Vol. 127, Part I, 1962, pp. 1406.

8. Parkes, E. W., "The Permanent Deformation of an Encastre Beam Struck Transversely at Any Point in Its Span," Proceedings of the Institute of Civil Engineers, Vol. 10, 1958, pp. 277.

9. Parkes, E. W., "The Permanent Deformation of a Cantilever Struck Transversely at Its Tip," Proceedings, Royal Society of London, England, Series A, Vol. 228, 1955, pp. 462.

10. Rogers, G. L., An Introduction to the Dynamics of Framed Structures, John Wiley and Sons, Inc., New York, N.Y., 1953.

11. Timoshenko, S., Vibration Problems in Engineering, New York: D. Van Nostrand Company, Inc., 1928.

12. Ting, Thomas C. T., and Symonds, P. S., "Impact of a Cantilever Beam with Strain Rate Sensitivity," Technical Report No. 73, Division of Applied Mathematics, Brown University, Providence, R.I., January 1962, Presented at Fourth U.S. National Congress of Applied Mechanics, June 18-21, 1962.

13. Wen, Robert K., and Toridis, Teoktistos, "Discrete Dynamic Models of Elasto-Inelastic Beams," Journal of the Engineering Mechanics Division, ASCE, Vol. 90, No. EM5, Proceedings Paper 4081, October 1964, pp. 71.

14. Wen, R. K., and Janssen, John G., "Dynamic Analysis of Elasto-Inelastic Frames," Proceedings of the Third World Conference on Earthquake Engineering, New Zealand, February, 1965.

APPENDIX

EXACT ELASTIC SOLUTION

To consider the reliability of the discrete model, a problem for which an exact solution is obtainable was solved. This solution was used for purposes of comparison in section 4.2 and Figure 4.5.

The problem consists of finding the elastic response of a uniform cantilever beam subjected to a suddenly applied distributed uniform load as shown in Figure 4.1a. Rogers' (10) gives the general equation for the normal mode shape of an elastic beam:

$$X(x) = C_1 \sin \lambda x + C_2 \sinh \lambda x + C_3 \cos \lambda x + C_4 \cosh \lambda x \tag{A1}$$

where

$$\lambda = mp^2/EI \tag{A2}$$

and p is the natural circular frequency. For a cantilever beam, the boundary conditions are given by:

$$\left.\begin{aligned} X(0) &= 0 \\ X'(0) &= 0 \\ X''(L) &= 0 \\ X'''(L) &= 0 \end{aligned}\right\} \tag{A3}$$

By introducing these boundary conditions into equation (A 1), the frequency equation and the normal mode shape may be determined.

The frequency equation is:

$$-\cos \lambda L \cosh \lambda L = 1 \tag{A4}$$

The eigen values, given by Timoshenko (11), are:

$\lambda_1 L = 1.875 \qquad \lambda_2 L = 4.694$
$\lambda_3 L = 7.855 \qquad \lambda_4 L = 10.996$
$\lambda_5 L = 14.137 \qquad \lambda_6 L = 17.279$
$\lambda_7 L = 20.420 \qquad \lambda_8 L = 23.562$
$\lambda_9 L = 26.704 \qquad \lambda_{10} L = 29.845$

The nth mode shape is:

$$X_n(x) = C_n \left[\frac{\sin \lambda_n x - \sinh \lambda_n x}{\cos \lambda_n L + \cosh \lambda_n L} + \frac{\cos \lambda_n x - \cosh \lambda_n x}{\sin \lambda_n L - \sinh \lambda_n L}\right] \tag{A5}$$

where C_n is a constant.

For forced vibration the equation of motion is given by

$$EI \frac{\partial^4 y}{\partial x^4} + m \frac{\partial^2 y}{\partial t^2} = w(x, t) \tag{A6}$$

The solution may be written in the form:

$$y(x, t) = \sum_{n=1}^{\infty} X_n(x) \psi_n(t) \tag{A7}$$

where ψ_n is the nth generalized coordinate. By orthogonality of the X_n's,

$$\int_0^L X_n(x) X_m(x)\, dx = 0 \qquad m \neq n \tag{A8}$$

If the modes are normalized, i.e.,

$$\int_0^L X_n^2(x)\, dx = 1 \tag{A9}$$

the value of C_n may be determined from:

$$C_n^2 = (L/4)^{-1} \left[\frac{\sin \lambda_n x - \sinh \lambda_n x}{\cos \lambda_n L + \cosh \lambda_n L} + \frac{\cos \lambda_n x - \cosh \lambda_n x}{\sin \lambda_n L - \sinh \lambda_n L}\right]^{-1}_{x = L} \tag{A10}$$

Inserting (A7) into (A6) and multiplying the resulting equation by

$X_m(x)$ the following results will be obtained.

$$EI \sum_{n=1}^{\infty} \psi_n(t) \cdot X_n'''' \cdot X_m + m \sum_{n=1}^{\infty} \ddot{\psi}_n(t) \cdot X_n \cdot X_m = X_m \cdot w(x,t) \qquad \text{(A11)}$$

Introducing the following identity for a prismatic beam

$$X_n'''' = \frac{p_n^2\, m\, X_n}{EI} \qquad \text{(A12)}$$

and integrating the entire equation over the length of the beam the following equation results.

$$p_n^2\, m\, \psi_n(t) + m\ddot{\psi}_n(t) = \int_0^L X_m\, w(x,t)\, dx \qquad \text{(A13)}$$

If $w(x,t)$ is a function of t alone, for example, a uniform load, integrating X_m over the length of the beam, the preceding equation becomes

$$\ddot{\psi}_n(t) + p_n^2 \psi_n(t) = \frac{w(t)\, C_n}{\lambda_n m} \left[\frac{2 - \cos\lambda_n L - \cosh\lambda_n L}{\cos\lambda_n L + \cosh\lambda_n L} + 1\right] \qquad \text{(A14)}$$

If $w(t)$ has the form of ce^{-rt} and writing

$$G_n = \frac{c\, C_n}{\lambda_n m} \left[\frac{2 - \cos\lambda_n L - \cosh\lambda_n L}{\cos\lambda_n L - \cosh\lambda_n L} + 1\right] \qquad \text{(A15)}$$

equation (A14) becomes

$$\ddot{\psi}_n(t) + p_n^2 \psi_n(t) = G_n\, e^{-rt} \qquad \text{(A16)}$$

The solution to (A16) can be shown to be

$$\psi_n(t) = A_n \cos p_n t + B_n \sin p_n t + \frac{G_n\, e^{-rt}}{(p_n^2 + r^2)} \qquad \text{(A17)}$$

For the initial conditions:

$$y(x, 0) = 0$$
$$\dot{y}(x, 0) = 0 \tag{A18}$$

the corresponding initial conditions for the variables ψ_n (for all n) are given by

$$\psi_n(0) = 0$$
$$\dot{\psi}_n(0) = 0 \tag{A19}$$

The values of A_n and B_n corresponding to the above initial conditions are:

$$A_n = -G_n/(p_n^2 + r^2)$$
$$B_n = r\,G_n/(p_n^2 + r^2) \tag{A20}$$

Thus ψ_n can be calculated from Equations (A17), (A20), and (A15). The modes X_n are determined from Equations (A5) and (A10). Finally, the dynamic deflections of the beam are calculated from Equation (A7). For the numerical problem solved ten modes were used in the sum that appears in Equation (A7).

Table (1) Comparison of Permanent End Slope of Cantilever Beams (in Degrees)

Material	From Tables #3 and 4 of Reference (1)							Discrete Model		
	Sample No.	$Q^* = \frac{I_o^2/2G}{M_o^2 L/2EI}$	Rigid Perfectly Plastic			Experimental Data		R = 0	R = 0.01	R = 0.04
			Rate Dependent		Rate Insensitive					
			Symonds	Ting						
Steel	E4	16	56	59	71	52		80	-	52
	F1	11.5	63	66	71	64		91	-	62
	F8	9.0	41	44	40	43		66	-	49
Aluminum	G1	7.9	43	44	47	34		49	43	-
	G3	8.6	59	59	59	51		59	51	-
	H4	3.2	66	-	66	57		70	62	-
	H9	3.6	27	28	24	24		32	30	-

*The symbol Q here corresponds to R used in Reference (1).

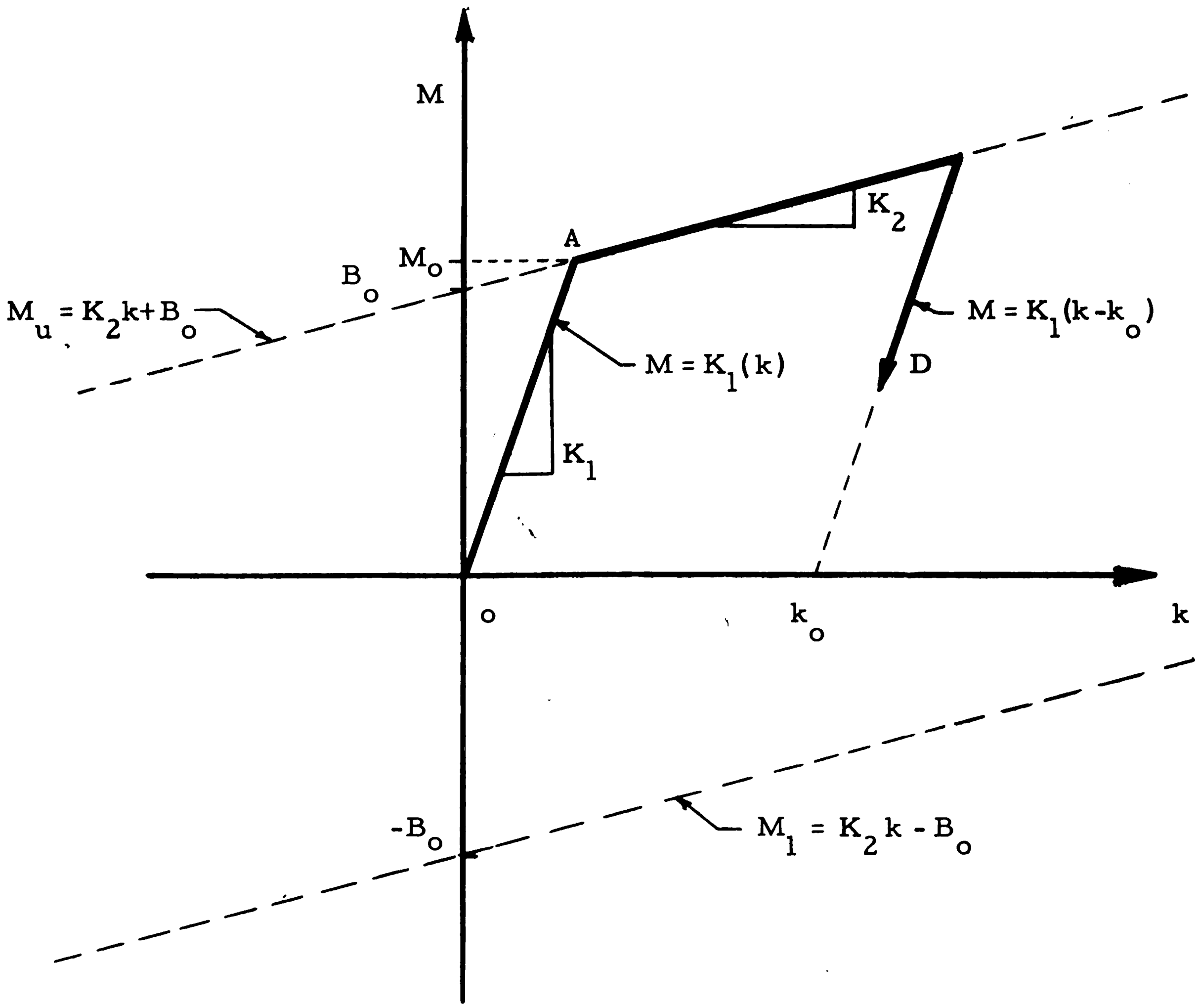

Figure 2.1 Moment Curvature Diagram for "Static" Loading.

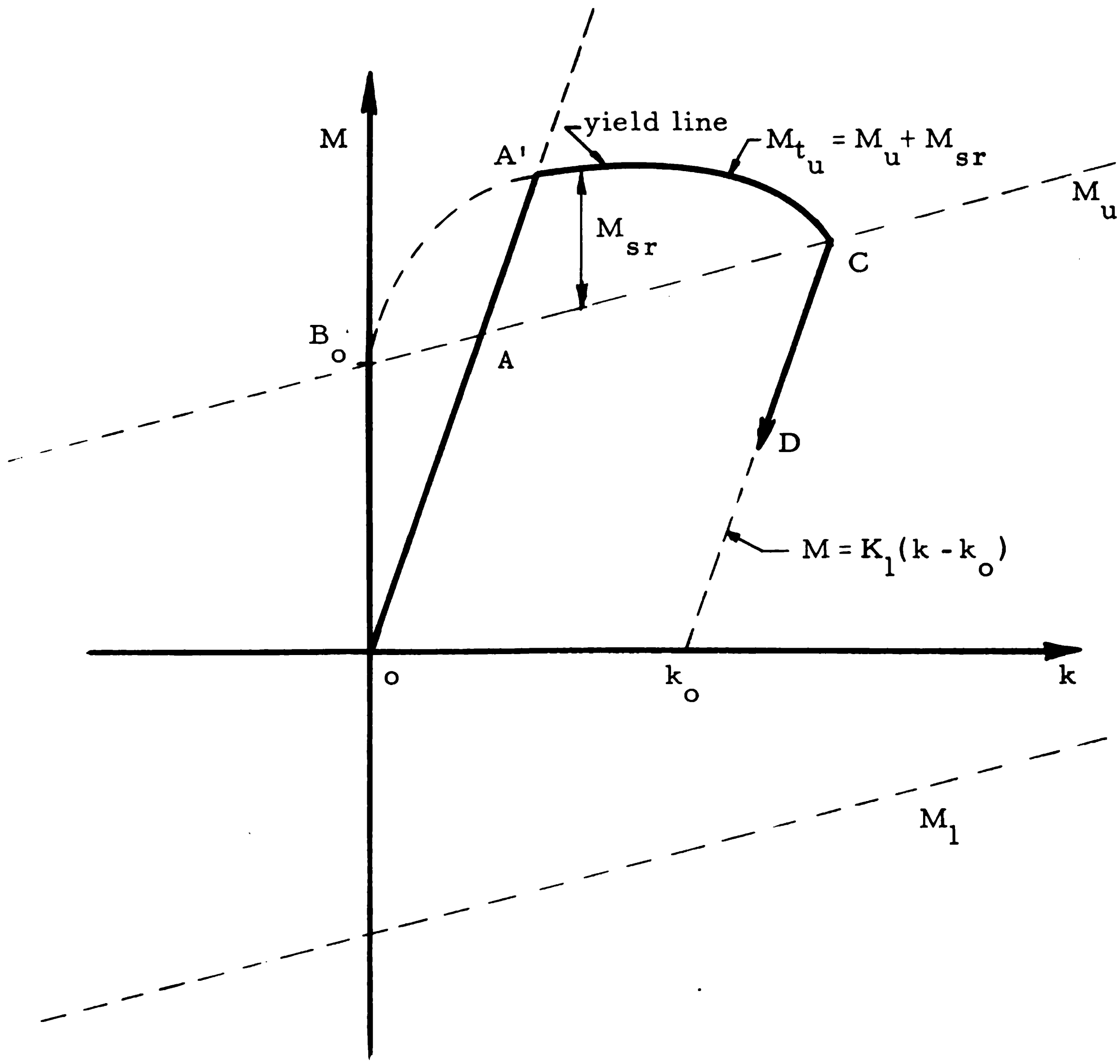

Figure 2.2 Moment Curvature Diagram with Strain Rate Effects Incorporated

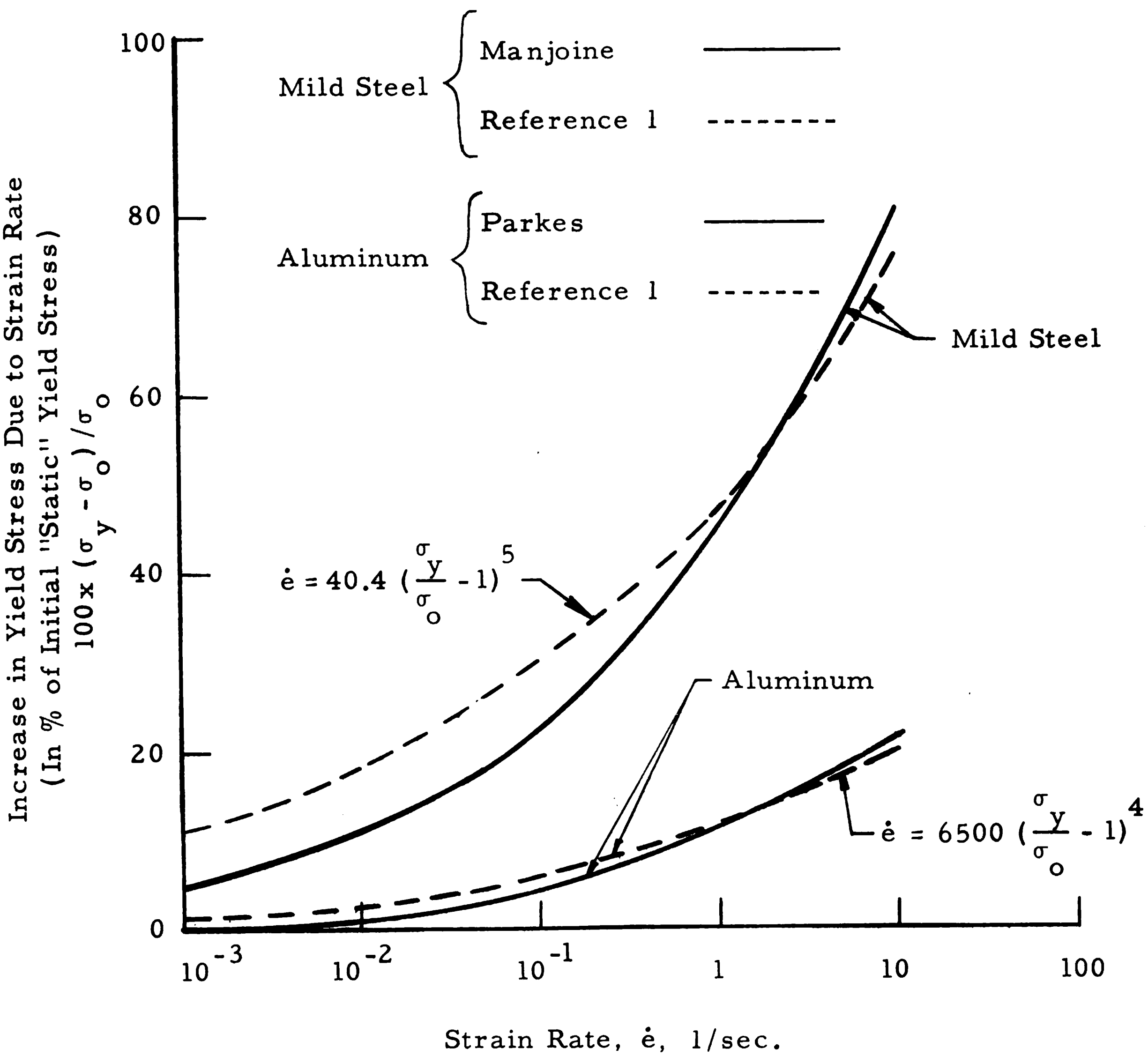

Figure 2.3 Effect of Strain Rate on Yield Stress

a)

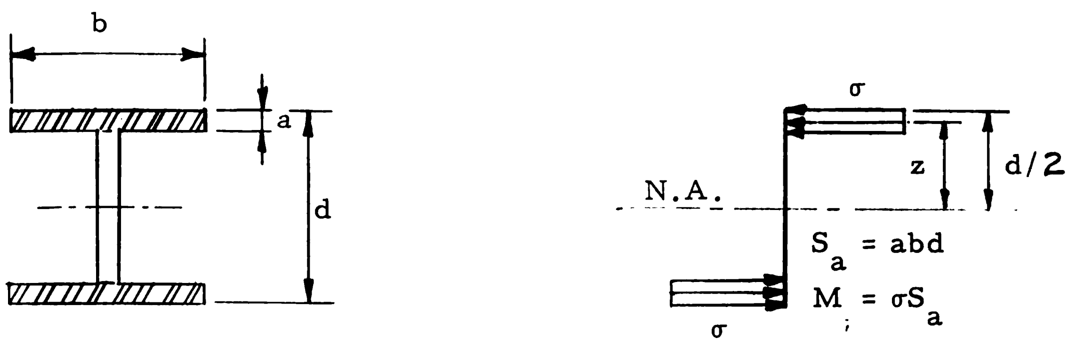

Only Flanges Considered Effective in Resisting Bending

Constant Stress Distribution in Flanges

Section Properties

$a = 0.748$ in.

$b = 10.117$ in

$d = 10.38$ in

$S_e = 73.7\ \text{in}^3$

$S_a = 78.5\ \text{in}^3$

$S_p = 82.8\ \text{in}^3$

Material Properties

$\sigma_y = 30,000$ psi

$E = 30,000,000$ psi

b)

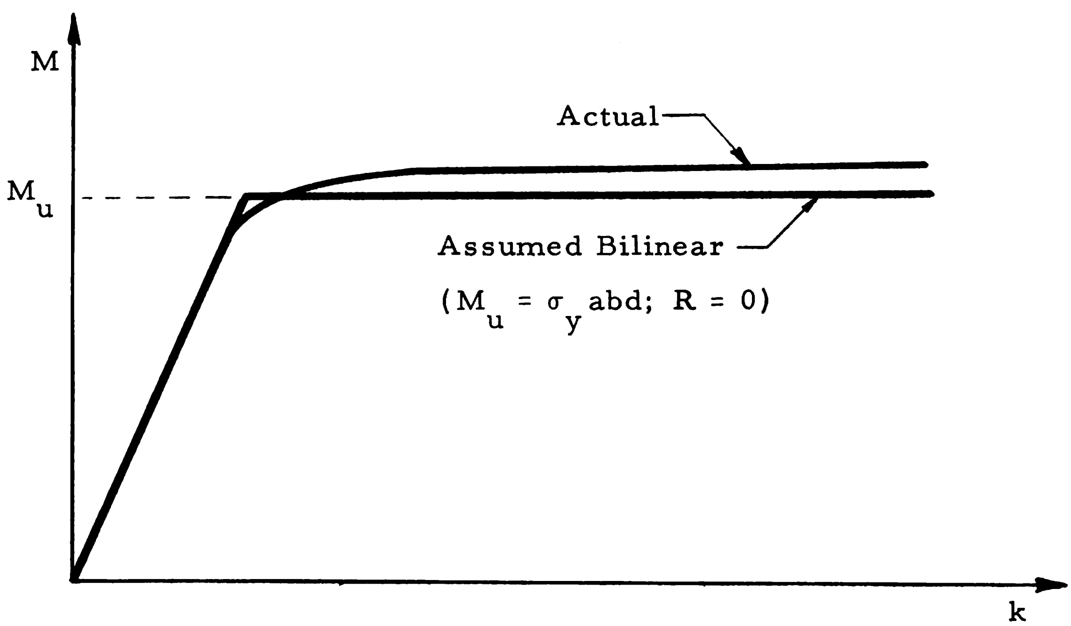

Figure 2.4 "Static" Moment Curvature Diagram for a 10 WF66

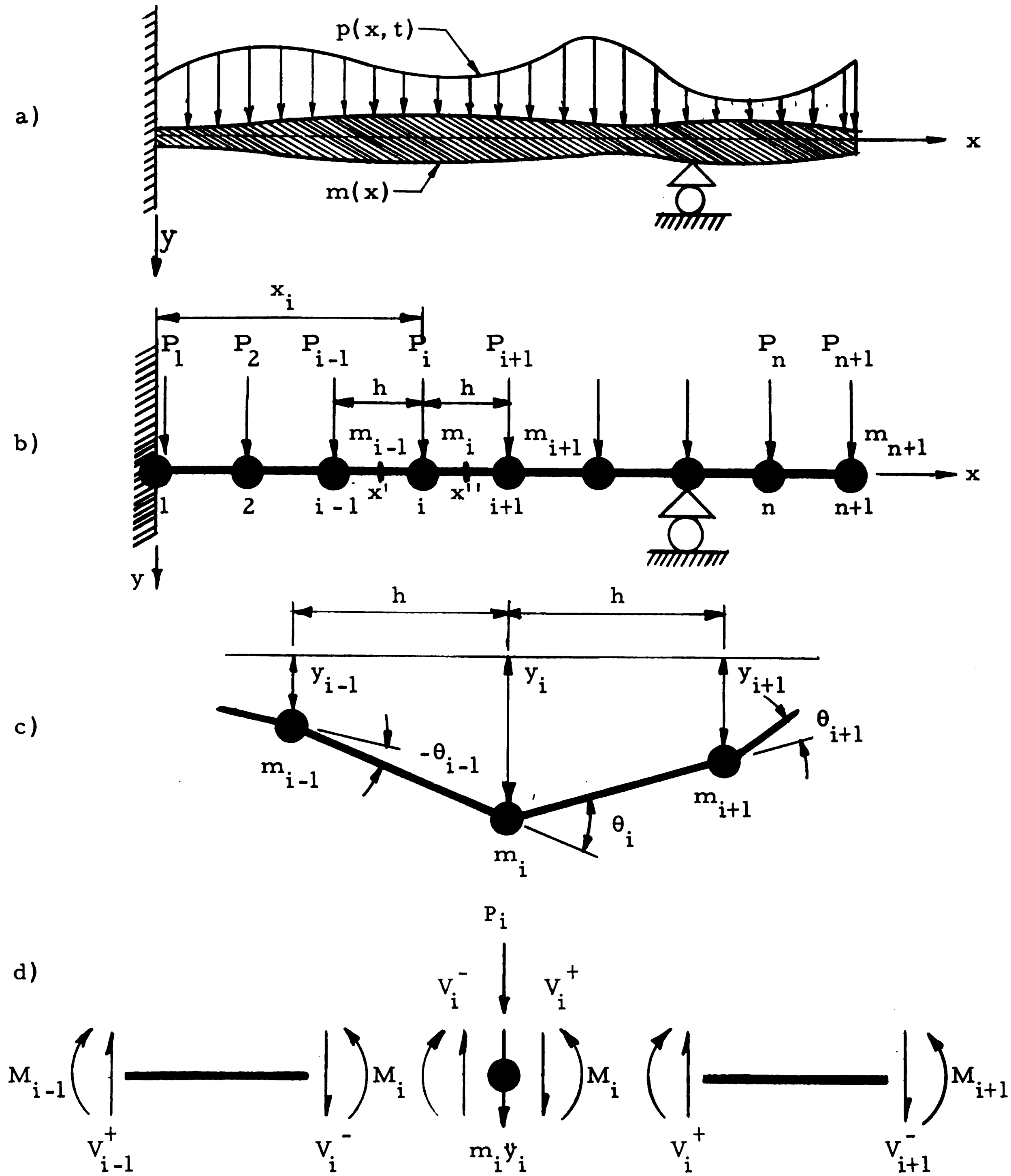

Figure 3.1 Beam Discretization

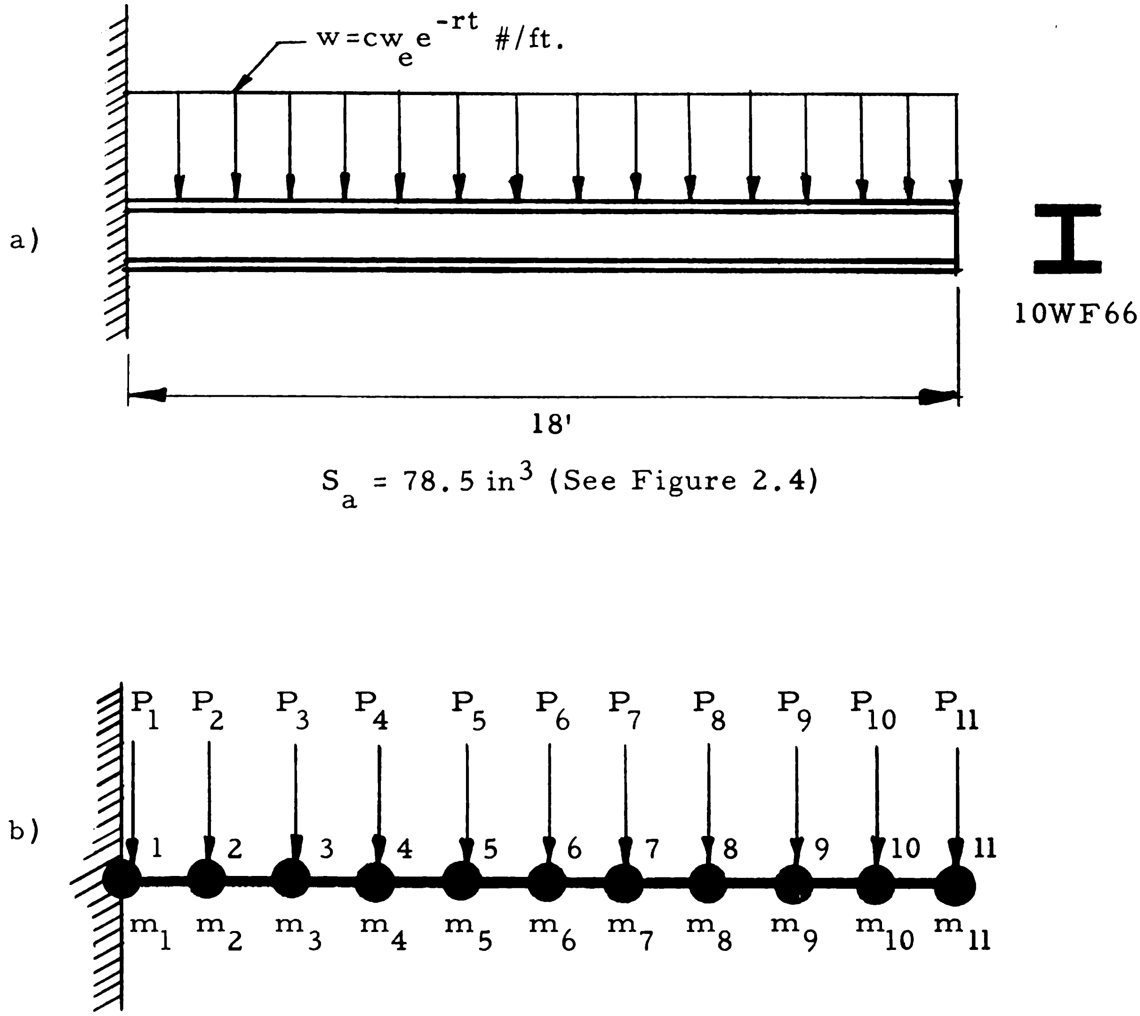

Figure 4.1 Prototype Cantilever Beam and Corresponding Discrete Model

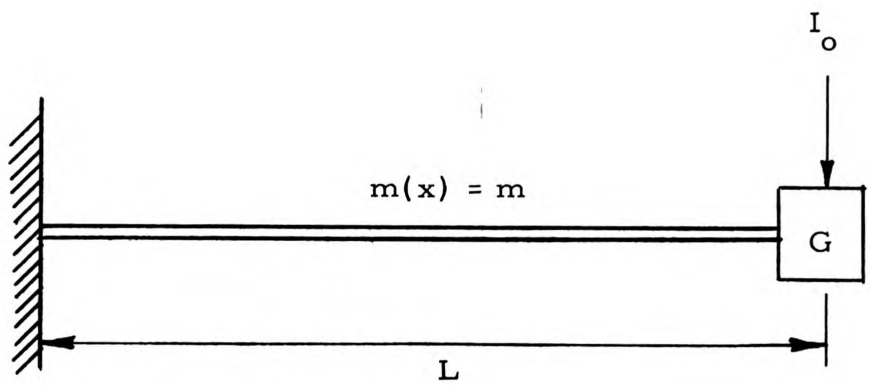

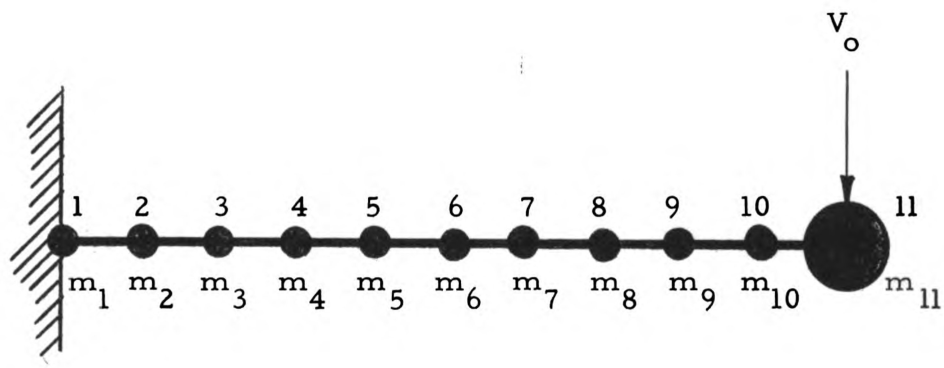

Figure 4.2 Prototype Cantilever Beam with Tip Mass Subjected to Impulsive Load and Corresponding Discrete Model

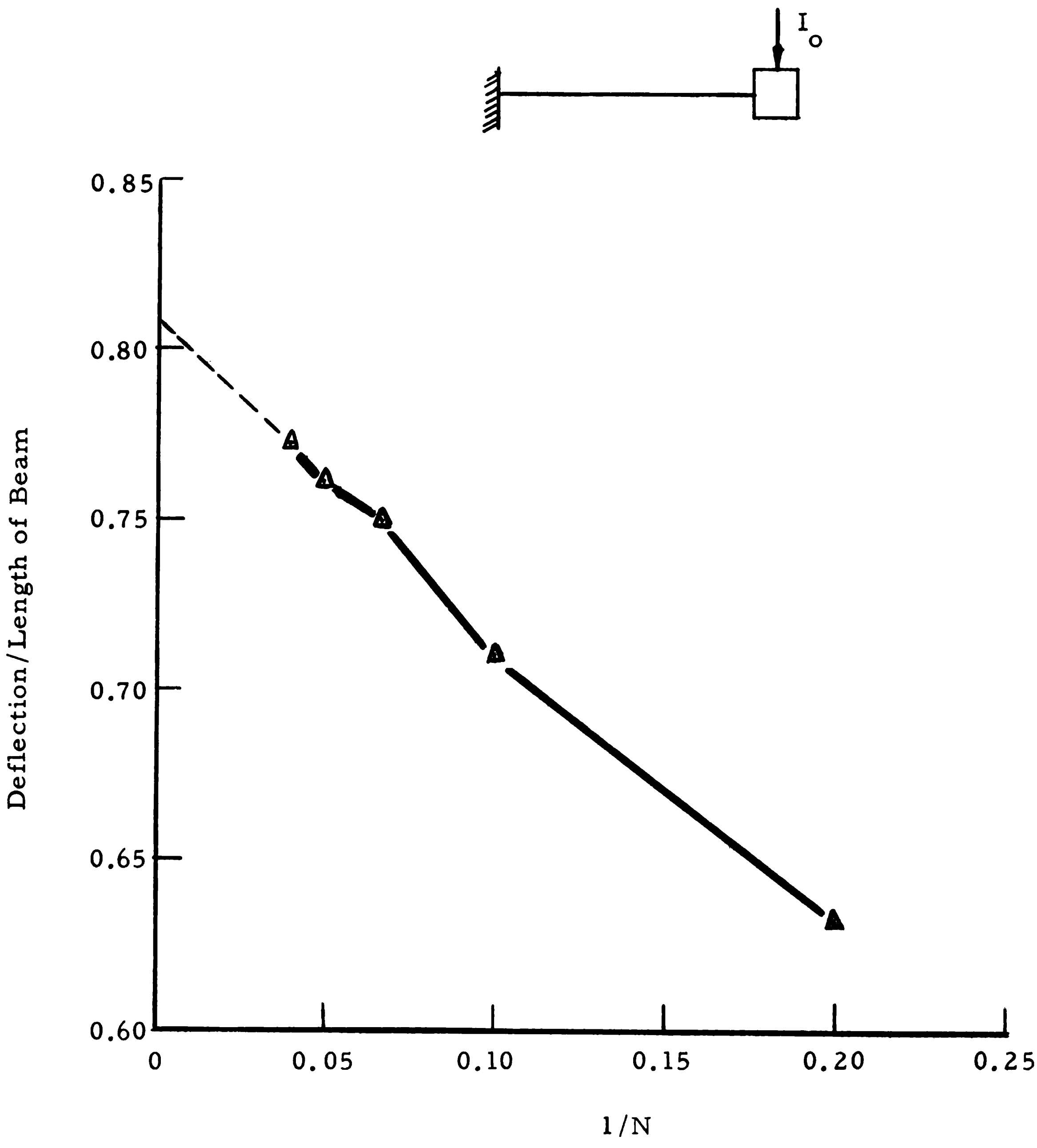

Figure 4.3 Convergence of Maximum Tip Deflection for R = 0

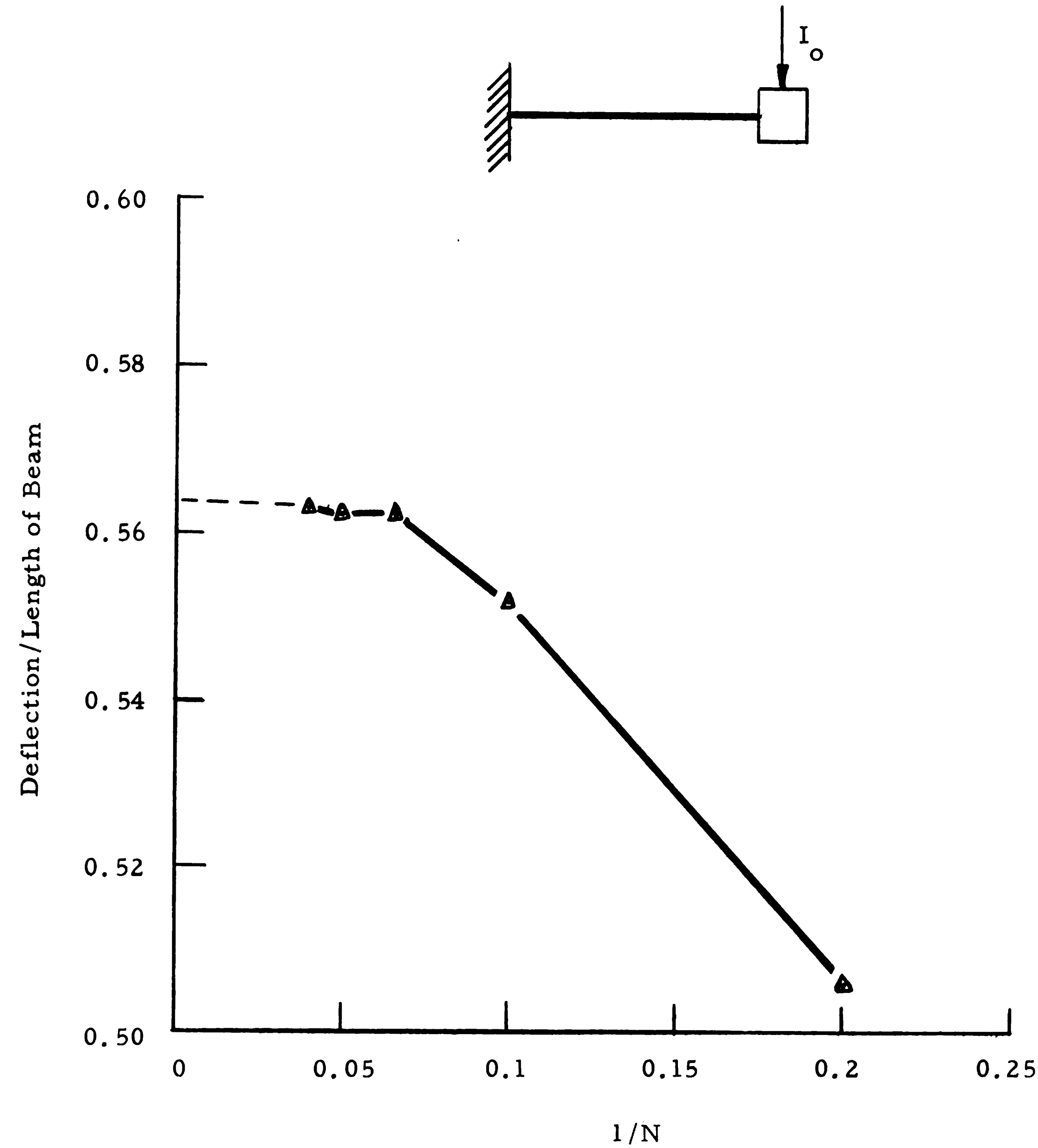

Figure 4.4 Convergence of Maximum Tip Deflection for R = 0.1

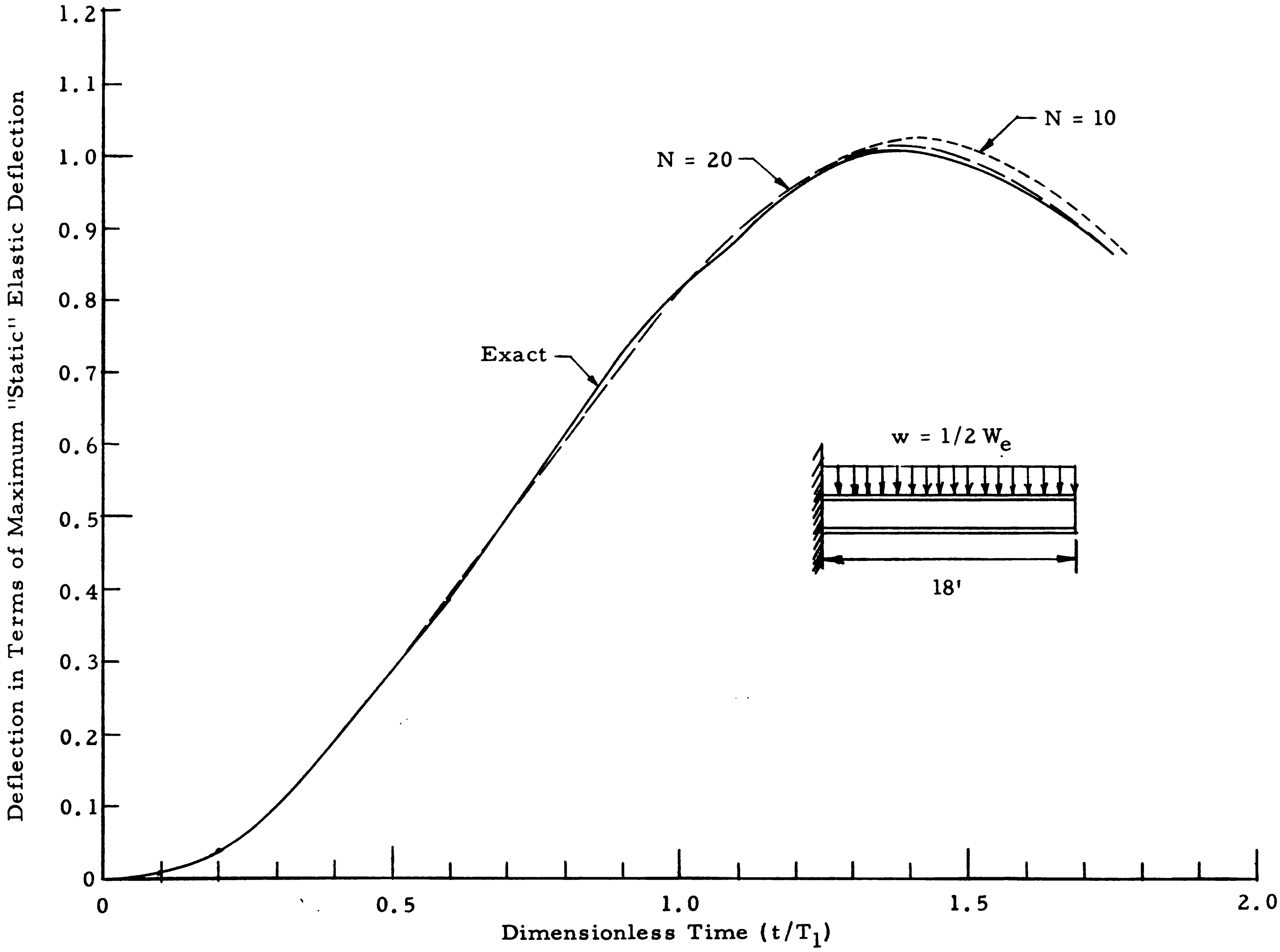

Figure 4.5 Comparison of Response History Curves

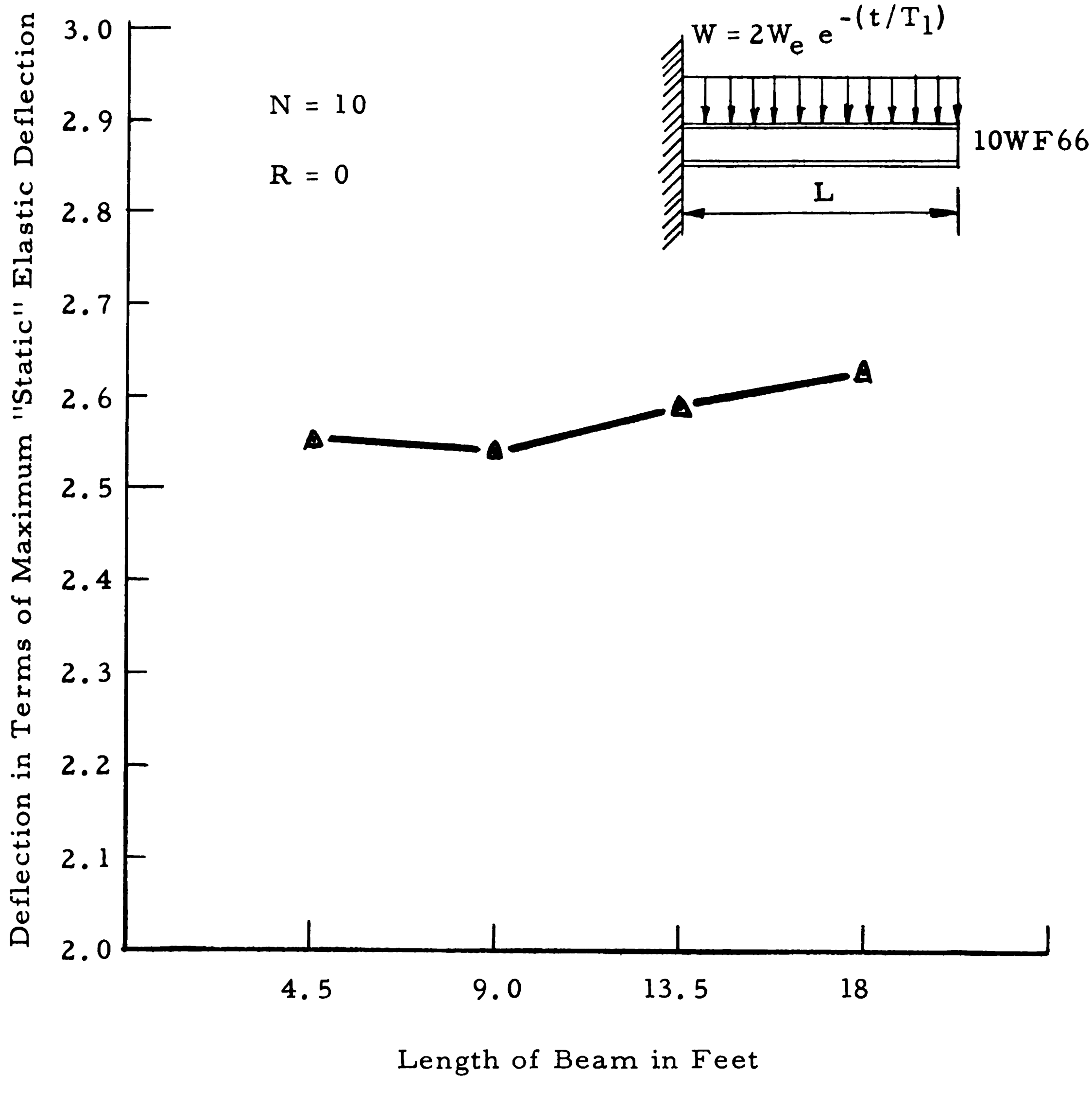

Figure 4.6 Maximum Tip Deflection for 10WF66 of Various Lengths (R=0)

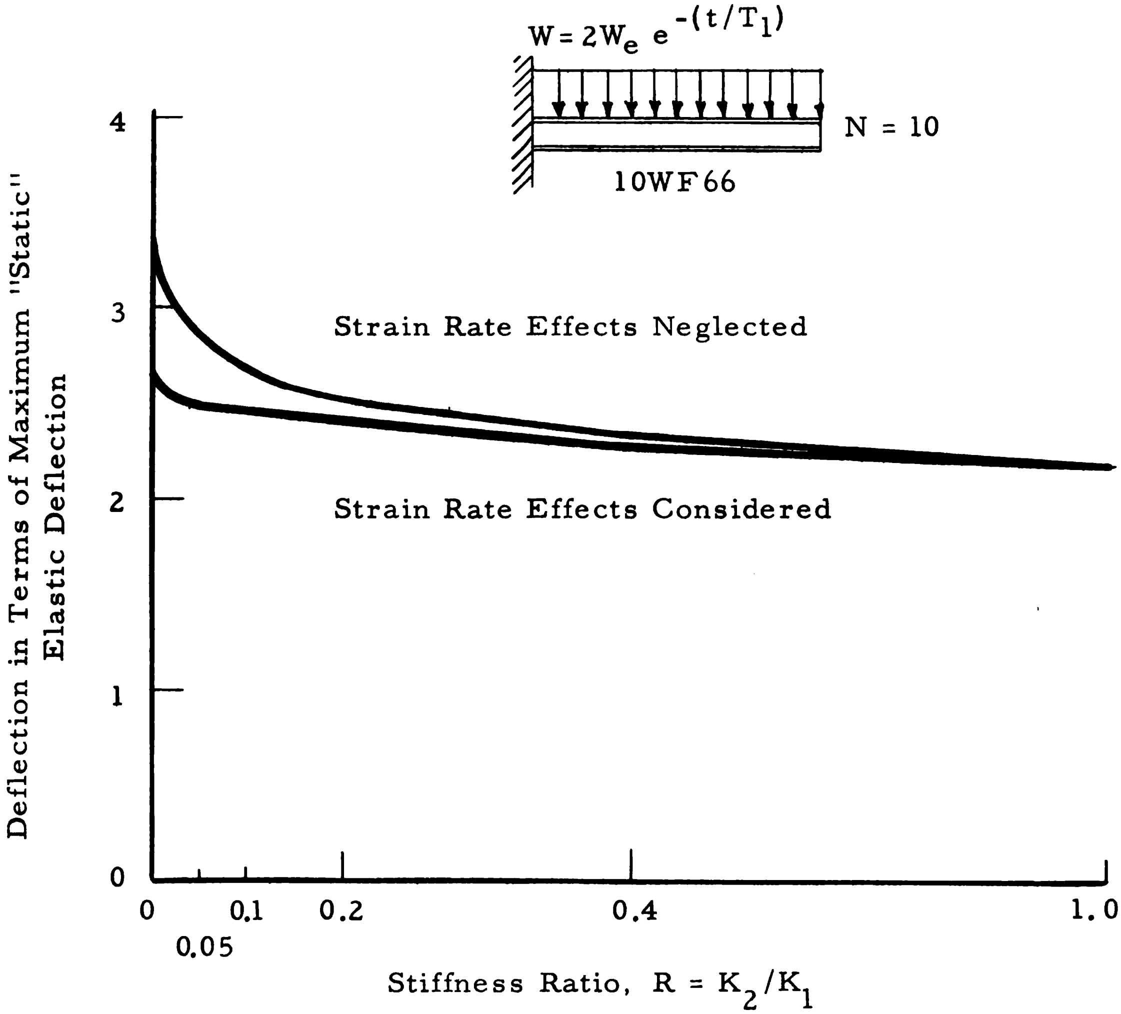

Figure 4.7 Effect of Strain Rate in the Presence of Strain Hardening

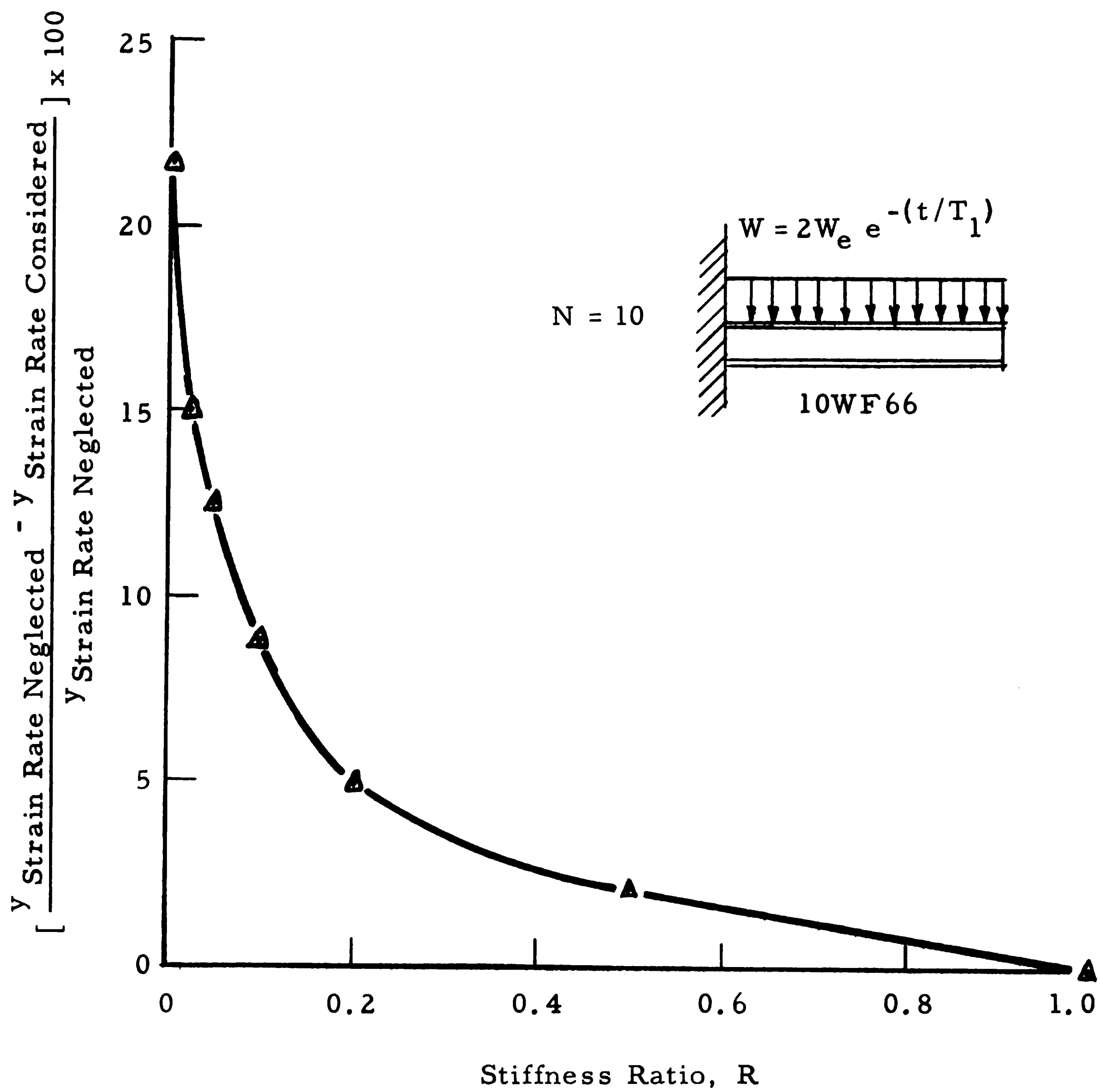

Figure 4.8 Percent Reduction of Maximum Deflection Due to Strain Rate for Various Values of R

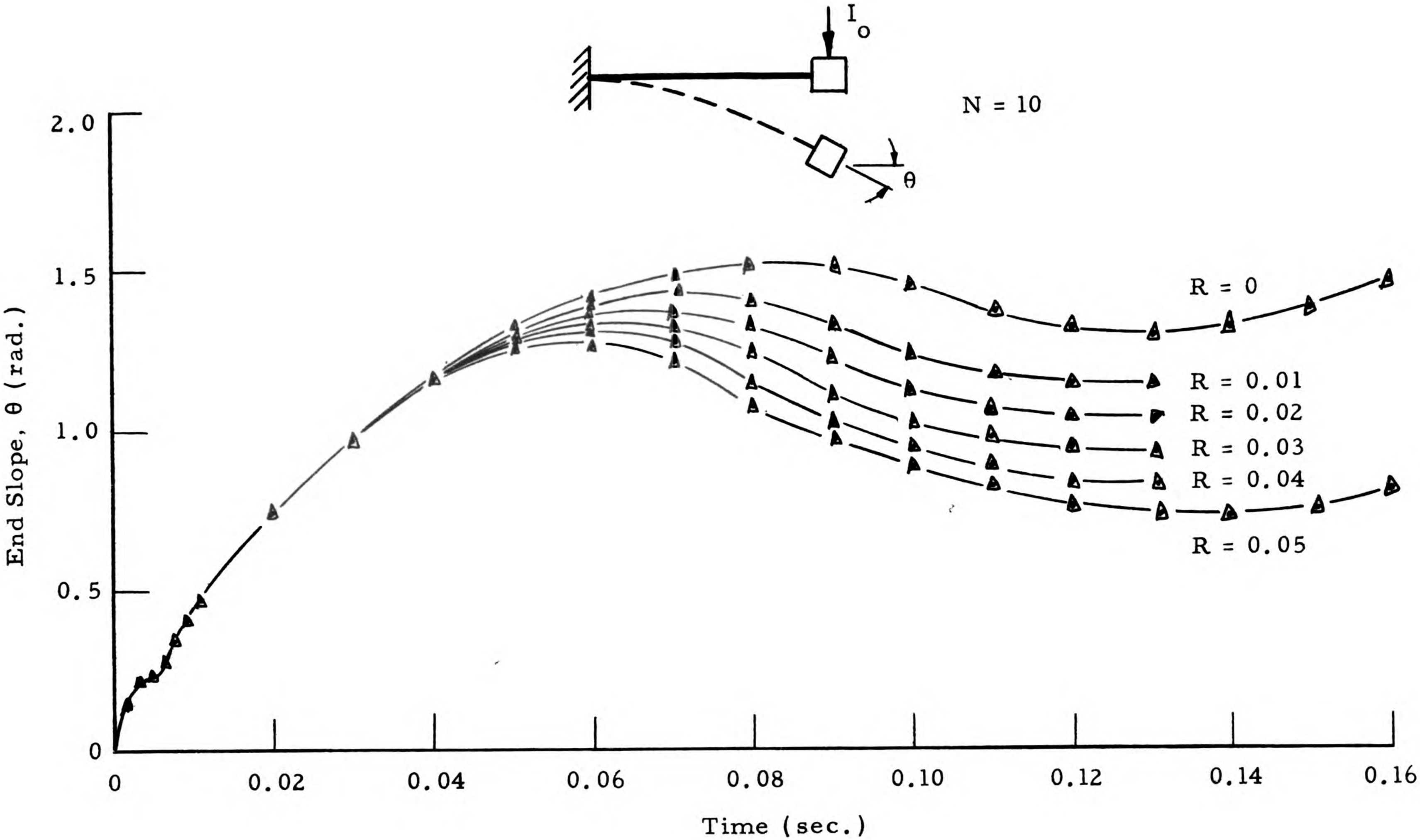

Figure 4.9 Response History Curves for Various Values of R

a)

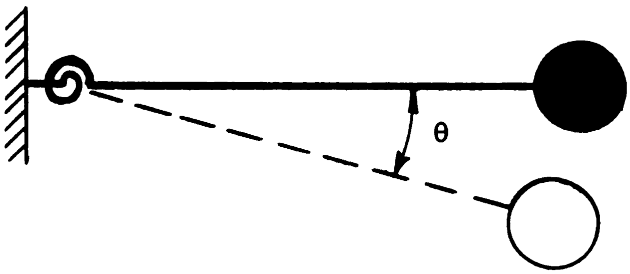

Simple One-Degree Freedom Structure

b)

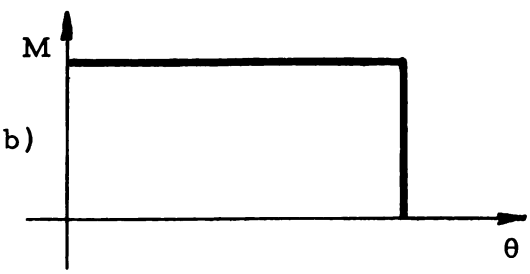

Rigid Perfectly Plastic

c)

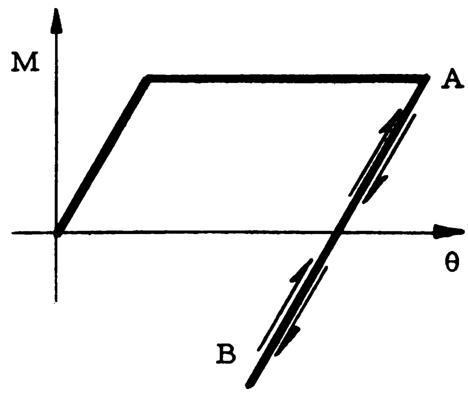

Elasto-Perfectly Plastic

d)

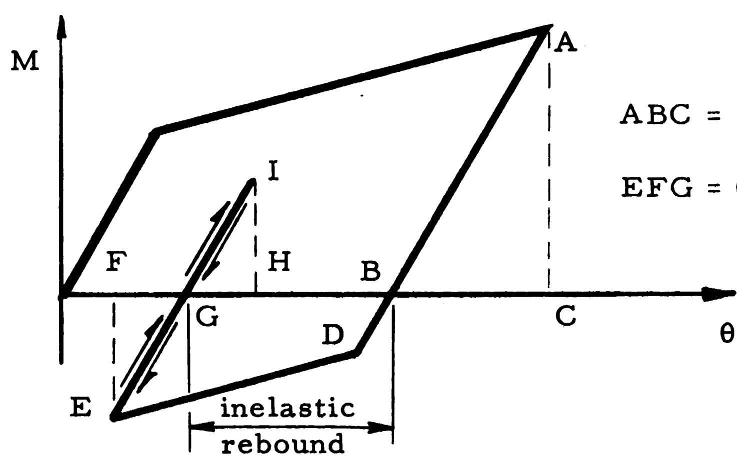

Elastic Strain Hardening

Figure 5.1 Behavior of Simple Structures with Different Moment Rotation Relations

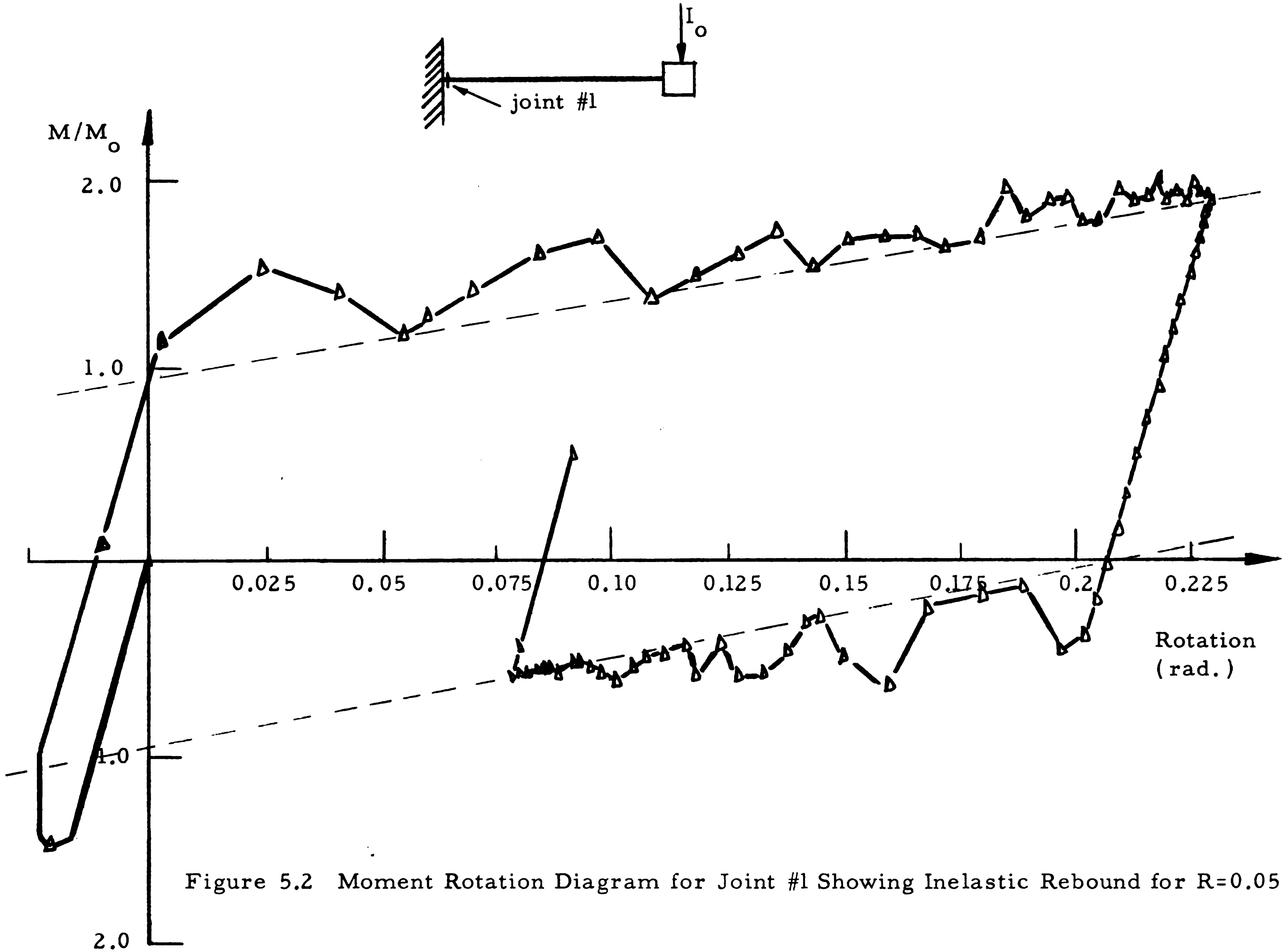

Figure 5.2 Moment Rotation Diagram for Joint #1 Showing Inelastic Rebound for R=0.05

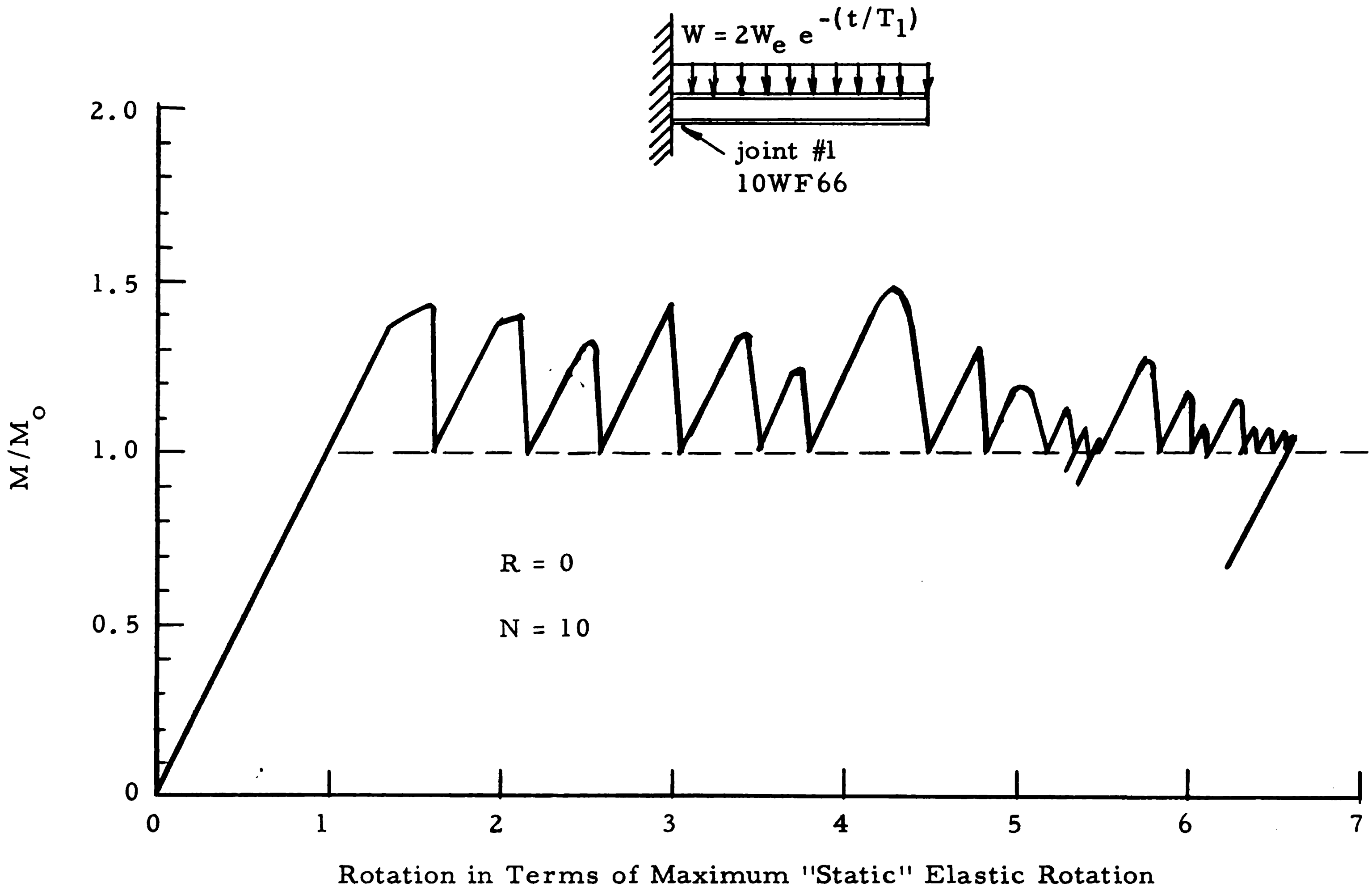

Figure 5.3 Effect of Higher Modes on Moment Rotation Diagram for Joint #1